GALAXY GROUPS AT INTERMEDIATE REDSHIFT

R. G. CARLBERG,[1,2] H. K. C. YEE,[1,2] S. L. MORRIS,[1,3] H. LIN,[1,2,4,5] P. B. HALL,[1,2,6]
D. R. PATTON,[1,2,7] M. SAWICKI,[1,2,8] AND C. W. SHEPHERD[1,2]

ABSTRACT

Galaxy groups likely to be virialized are identified within the CNOC2 intermediate-redshift galaxy survey. The resulting groups have a median velocity dispersion, $\sigma_1 \simeq 200$ km s^{-1}. The virial mass–to–light ratios, using k-corrected and evolution-compensated luminosities, have medians in the range of 150–250 h $M_\odot/L_\odot$, depending on group definition details. The number–velocity dispersion relation at $\sigma_1 \gtrsim 200$ km s^{-1} is in agreement with the low-mass extrapolation of the cluster-normalized Press-Schechter model. Lower velocity dispersion groups are deficient relative to the Press-Schechter model. The two-point group-group autocorrelation function has $r_0 = 6.8 \pm 0.3$ h^{-1} Mpc, which is much larger than the correlations of individual galaxies, but about as expected from biased clustering. The mean number density of galaxies around group centers falls nearly as a power law with $r^{-2.5}$ and has no well-defined core. The projected velocity dispersion of galaxies around group centers is either flat or slowly rising outward. The combination of a steeper than isothermal density profile and the outward rising velocity dispersion implies that the mass-to-light ratio of groups rises with radius if the velocity ellipsoid is isotropic but could be nearly constant if the galaxy orbits are nearly circular. Such strong tangential anisotropy is not supported by other evidence. Although the implication of a rising M/L must be viewed with caution, it could naturally arise through dynamical friction acting on the galaxies in a background of "classical" collisionless dark matter.

Subject headings: galaxies: evolution — large-scale structure of universe

On-line material: machine-readable table

1. INTRODUCTION

Small groups of galaxies are important cosmological indicators of the distribution and properties of the dark matter in the universe. They occupy the mass and velocity dispersion range between individual galactic halos and the large halos of rich galaxy clusters (Abell 1958; Burbidge & Burbidge 1961; Gott & Turner 1976; Hickson 1982; Ramella, Geller, & Huchra 1989; Nolthenius & White 1987). The rms velocity dispersion of groups overlaps that of individual high-luminosity galaxies. The velocities and positions of the group galaxies can be used to measure the properties of the group halos as individuals and as a population. Groups at intermediate redshift are suitable targets for X-ray observation and weak gravitational lensing studies that are complementary probes of their contents. Consequently, groups can be used to probe the properties of the dark matter on scales and at velocities much smaller than can be examined in galaxy clusters.

The theory of structure growth in the universe is based on the paradigm that the dark matter consists of collisionless particles that only interact via the gravitational force. Cold dark matter (CDM) is a specific form of this hypothesis that has been subjected to intensive theoretical study. A particular strength is that the properties of virialized halos can be predicted from a given density perturbation spectrum to full nonlinearity via simulations and various analytic approximations. These predictions have been tested with varying degrees of success against the dark matter halos of individual galaxies and rich clusters but are less examined on intermediate scales. The intermediate scales are interesting because they are at much higher phase-space densities than massive galaxy clusters, yet their central dark matter densities are not overwhelmed and altered by the baryonic matter, as is the case for most normal galaxies.

The CDM theory gives specific predictions of the statistical properties of the dark halo population and the mean internal properties of individual halos. The Press-Schechter (1974) theory predicts the number of halos as a function of mass or velocity dispersion. At low redshift, suitably selected groups have a population volume density in accord with the cluster-normalized Press-Schechter prediction (Moore, Frenk, & White 1993; Girardi & Giuricin 2000). A second global statistic is the clustering of dark matter halos that is predicted using analytic approximations that have been compared to n-body results (Mo & White 1996; Jing 1998). This biased "peaks" theory predicts a slow increase of clustering strength with halo mass. The internal density structure of the halos is found in simulations to have a power-law cusp, $r^{-1.0}$ to $r^{-1.5}$, which asymptotically steepens to approximately r^{-3} beyond the virial radius (Dubinski & Carlberg 1991; Navarro, Frenk, & White 1996, hereafter NFW96; Moore et al. 1999b; Avila-Reese et

al. 1999). The goal of this paper is to find a collection of virialized groups that can then be compared to the predictions of the global statistics and internal structure of intermediate-mass dark matter halos.

The paper is organized as follows. The next section describes our approach to identifying groups in a redshift catalog. Section 3 gives an overview of the Canadian Network for Observational Cosmology's field galaxy redshift survey (CNOC2) and the virialized groups that we find. In § 4 the number–velocity dispersion relation and the two-point correlation function are computed and compared to dark matter halo predictions. In § 5 we derive the group-galaxy two-dimensional cross-correlation function from which we measure the mean projected density distribution and projected velocity distribution. In § 6 we model these as projections of simple three-dimensional systems to derive the mean mass density profile and mass-to-light ratio as a function of radius, which leads to the discovery that groups have a rising mass-to-light ratio. We examine the rising mass-to-light ratio for various alternative samples to search for systematic trends that might point to its physical origin. We conclude with a discussion of the possible implications of these results and a short set of empirical conclusions. We use $H_0 = 100 \, h$ km s^{-1} Mpc^{-1} throughout this paper and adopt $\Omega_M = 0.2$, $\Omega_\Lambda = 0$ as our reference cosmological model. The distances and transverse lengths would be about 8% larger in an $\Omega_M = 0.3$, $\Lambda = 0.7$ cosmology at the median redshift.

2. FINDING GROUPS IN REDSHIFT SPACE

In redshift space there is a fundamental degeneracy between position and line-of-sight velocity. Consequently, the precise galaxy membership of a group found in redshift space is always a statistical issue. A group is defined here as a collection of three or more galaxies, above a fixed minimum luminosity, that meet a set of positional requirements designed to minimize chance associations. Here we specifically seek virialized groups, which are collapsed and hence quite dense compared to groups that are only required to be bound. The goal of identifying virialized groups motivates us to introduce a second step in the group search that is designed to identify the virialized subset of a redshift space group.

Most group search methods are based on the friends-of-friends (FOF) algorithm used by Huchra & Geller (1982). This is an important method that gives unique groups, independent of starting galaxy. The FOF algorithm can be tuned to yield groups of varying redshift space overdensity, but always with some ambiguity about group membership, which becomes more severe as the number of members declines (Frederic 1995a; Mahdavi et al. 1999, 2000). Galaxies in groups with velocity dispersions below about 200 km s^{-1} will have relatively short dynamical friction inspiral times. This implies that low-velocity dispersion groups are likely to have genuine dynamical distinctions, such as orbit and radial distributions of galaxies, in comparison to more massive groups (Diaferio et al. 1993). However, the FOF algorithm will reliably identify the groups independent of the importance of friction.

The FOF algorithm starts with any galaxy as the beginning of a trial group. All galaxies closer than some maximum distance (discussed below) are added to the group. Then, each of the new group members is in turn used as a center to search for its neighbors to add to the growing

group, continuing until no more sufficiently close new galaxies are found. Then one proceeds to a previously unexamined galaxy to try to start a new group. This process continues until all galaxies have been examined for neighbors. Groups of one and two are then deleted from the catalog. The FOF algorithm requires two parameters for redshift space group searches. These are a maximum separation in projected radius, r_p^{max}, and either a maximum separation velocity, Δv^{max}, or comoving redshift space distance difference, r_z^{max}, required to join the group. The Δv^{max} and r_z^{max} parameters are related through $\Delta v = H(z)r_z/(1+z)$. We use Δv selection for kinematic measurements and r_z selection for group finding. The r_p^{max} and r_z^{max} parameters need to be adjusted mutually to take into account the mean volume density of the galaxy survey, $n_g(z)$, so as to produce an overdensity with respect to the field chosen on the basis of an experimental goal with an allowance for redshift space blurring. The resulting galaxy overdensity in the cylindrical redshift space search volume is

$$\frac{\delta n}{n_0} \simeq \frac{1}{2\pi (r_p^{max})^2 r_z^{max} n_g(z)} . \tag{1}$$

The r_z^{max} parameter needs to be chosen in relation to r_p^{max} with some care.

Here we are interested exclusively in virialized groups, suggesting we devise a variant of the basic FOF algorithm that matches well to the techniques used for rich clusters of galaxies. In configuration space virialization demands a mean interior density of approximately $178\Omega^{0.45}\rho_c$ (Eke, Navarro, & Frenk 1998), equivalent to $\sim 350\rho_0$ in a low-density, flat cosmology. A conventional approximation is that such groups will be contained inside the radius r_{200}, which can be estimated from the virial theorem as $r_{200} = 3^{1/2}\sigma_1/[10H(z)]$, where σ_1 is the line-of-sight velocity dispersion and $H(z)$ is the Hubble constant at the redshift of interest (Carlberg et al. 1996). For a given σ_1 the virialized group members will be, on average, contained within approximately $1.5r_{200}$, if the mean density is falling like r^{-3}. The field pairwise velocity dispersion is approximately 300 km s^{-1} (Davis & Peebles 1983), equivalent to a single galaxy random velocity of about 200 km s^{-1}. This velocity dispersion is largely generated in galaxy groups, which suggests that an average r_{200} will be about 0.3 h^{-1} Mpc. In the redshift direction we seek to include galaxies out to about twice σ_1, although we explore a wider range of values. Similar considerations emerge on the basis of consideration of groups in n-body simulations (Nolthenius & White 1987; Frederic 1995a). Some of our results depend on the derived σ_1; however, many of them are only a function of the locations of the group centers, which are not very sensitive to the group selection procedure.

The FOF algorithm provides a set of trial groups whose properties are fixed by the input link distance parameters such that many of them may not be virialized. Virialized groups have a minimum overdensity of about $200\rho_c$. Hence, for each trial group we estimate a velocity dispersion that is then used to calculate r_{200}. Galaxies beyond a distance to the group center of $1.5r_{200}$ are discarded. The remaining galaxies are used to recalculate the velocity dispersion. This can be iterated until the group converges to a stable set. Some trial groups quickly drop to only one or two members and hence no longer qualify for group status. On the other hand, if we choose a very large starting value of r_p^{max} or
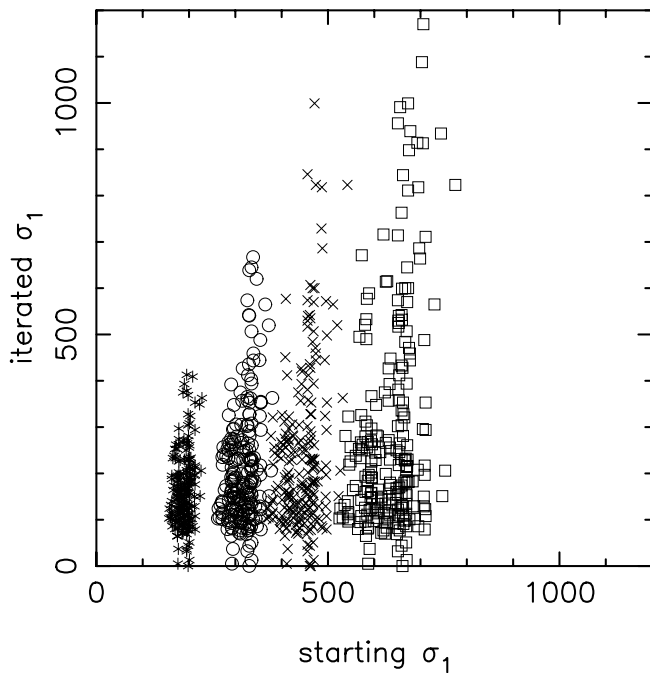
FIG. 1.—Line-of-sight velocity dispersion as estimated on the first pass (abscissa) of the group refinement and on the fourth pass (ordinate) for sets of group-finding parameters. The r_p^{max} is fixed at 0.25 h^{-1} Mpc. The asterisks, circles, crosses, and squares are for r_z^{max} of 3, 5, 7, and 10 h^{-1} Mpc, respectively.

Δv^{max}, a few groups will percolate over very large structures. A minor complication is that we must identify a group center.

The details of our group finding algorithm follow. (1) Pick a cosmology for the analysis ($H_0 = 100$ km s^{-1} Mpc^{-1}, $\Omega_M = 0.2$, $\Omega_\Lambda = 0$). (2) Set the sample's redshift and absolute luminosity limits (k-corrected and evolution-
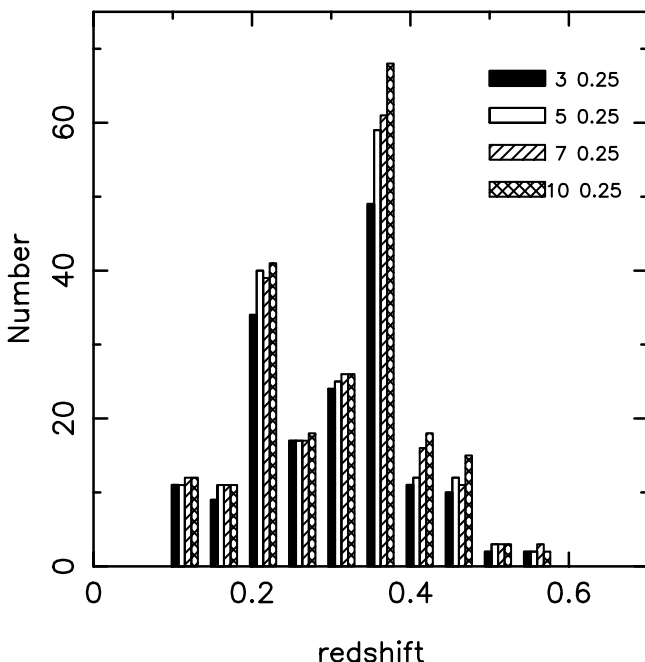

FIG. 2.—Redshift distribution of groups found with r_p^{max} fixed at 0.25 h^{-1} Mpc and r_z^{max} (upper right) varying over the same range as Fig. 1.

compensated at a mean rate of 1 mag per unit redshift) of $M_R^{ke} = -18.5$ mag (no initial redshift limits), which defines a galaxy sample for all further operations. (3) Pick an r_p^{max} (our standard groups use 0.25 h^{-1} Mpc) and r_z^{max} (5 h^{-1} Mpc for our standard groups). Center a cylinder of radius r_p^{max} and forward and backward extent of r_z^{max} on each sample galaxy and count the number of sample galaxies. To create a background estimate, we randomly draw points from an $n_g(z)$ fitted to the full sample and count the number within the sample cylinder. If the search radii initially give less than three neighbors, then multiply smoothing lengths by 1.5 and repeat for this sample galaxy. On the basis of these densities we define a new subsample of galaxies eligible to be group members based on the requirement that the local overdensity exceed some specified minimum value. In this paper we only require that the local overdensity be positive. (4) Select the highest density ungrouped galaxy and begin to find a new group. (5) Standing on each new group member in turn, add to the group any galaxy in the minimum overdensity subsample that is closer than r_p^{max} and r_z^{max}. Repeat this step until no new galaxies are added. (6) This FOF group defines the starting group for the virialized group iteration. (7) For the trial virialized group, determine the geometric selection function–weighted mean x, y, z and σ_1. Trim galaxies beyond, or add galaxies from the FOF list within, $r_p = 1.5 r_{200}$ and $\Delta v = 3\sigma_1$. Repeat step 7 four more times, requiring that the last two iterations have an identical result. (8) Drop single galaxies and pairs from the catalog.

3. GROUPS IN THE CNOC2 SURVEY

The Canadian Network for Observational Cosmology Field Galaxy Redshift Survey (CNOC2) was undertaken primarily to study the dynamics of galaxy clustering at intermediate redshift. The survey methods and catalogs are fully described in Yee et al. (2000). The survey covers a total of about 1.5 deg^2 in four patches spread around the sky for observing efficiency and to control cosmic variance. Galaxy redshifts are obtained over the redshift range 0–0.7, with the unbiased spectroscopic sample extending between redshifts 0.1 and 0.55 (Yee et al. 2000). The catalogs contain approximately 6000 galaxy redshifts with an accuracy between 70 and 100 km s^{-1}, along with *UBVRI* photometry. The groups are constructed from these cataloged galaxies. The luminosity and clustering evolution of the sample as a whole has been previously discussed (Lin et al. 1999; Carlberg et al. 2000).

The CNOC2 sample is not spectroscopically complete; however, the selection function is very well defined on the basis of the large and deep underlying photometric sample (Lin et al. 1999; Yee et al. 2000). The survey's average redshift completeness is about 45%, with nearly 100% completeness 3 mag above the limit and about 20% at the limit. Within our primary redshift range, 0.10–0.55, the redshift completeness to the flux limit is higher than for the sample as a whole. From our luminosity functions (Lin et al. 1999) we calculate that about 75% of the galaxies will have a redshift within our primary redshift range (Yee et al. 2000). Accordingly, about 60% of the galaxies above the flux limit in the redshift range 0.1–0.55 have measured redshifts. If a group contains three galaxies within the survey limits, then the probability from the cumulative binomial distribution that we will obtain three redshifts is $(0.6)^3$ or 0.216. If the group contains four eligible galaxies, then the probability

we will obtain three or more redshifts rises to 0.47. The probabilities of obtaining three or more redshifts in groups of five, six, seven, and eight eligible members are 0.68, 0.81, 0.90, and 0.95, respectively, assuming no further reduction in completeness due to slit crowding (Yee et al. 2000). Our average group contains 3.8 galaxies with redshifts. We conclude that our roughly one-in-two sampling allows us to detect about half of the three or more member groups that are present. This level of completeness has no bearing on most of our analysis, so we normally do not attempt to compensate for this effect. Of the 3290 galaxies above our sample limits, we find that 21% are placed into our "standard" virialized groups, similar to the 25% found in LCDM simulations (Diaferio et al. 1999).

There is a small incompleteness due to groups at the boundaries of the surveyed region. Examining a typical field, we find that no more than 20% of the groups have any of their r_{200} area beyond the boundary and none are missing as much as one-half. Therefore, we estimate that approximately 10% of the group members are "missing," which will lead to errors that are small relative to the random errors for these small groups.

The only two parameters that turn out to have much of an impact on the groups are r_p^{max} and r_z^{max}. Our $200\rho_c$ density requirement forces the "raw" groups to have a velocity dispersion strongly correlated with the search distance in the redshift direction, r_z^{max}. The effect of the iteration on the group velocity dispersion is shown in Figure 1. The initial velocity dispersion is calculated for the FOF groups and is hence very strongly correlated with the chosen r_z^{max}. The iteration to find virialized groups allows the σ_1 values to relax to more appropriate values. However, some less than ideal groups do persist, which will lead us continually to consider alternate samples throughout this paper. Most of the groups converge to a stable membership in one or two iterations, with only 1%–2% discarded as a result of failure to converge in four iterations.

Figure 2 shows the redshift distribution of the groups for four group catalogs with increasing r_z^{max}. Beyond redshift 0.45 the sample becomes incomplete as the flux limit of $m_R = 21.5$ mag causes galaxies to slip below the sample absolute magnitude limit $M_R^{ke} = -18.5$ mag. Both this figure and a detailed examination of the lists of groups show that the sets of groups have a large overlap, independent of the search parameters. That is, this indirectly indicates that the set of group centers is relatively insensitive to the group finding procedure. In the next section we examine a variety of statistics to form a basis to select some group catalogs as best suited to various analyses.

4. GLOBAL PROPERTIES OF GROUPS AND HALOS

We will use three global properties of the groups to assess the degree of correspondence of various group catalogs to dark halos. These are the mass-to-light ratio distribution, the abundance as a function of velocity dispersion, and the clustering properties. The virial mass–to–R-band light ratio, M_{VT}/L_R, of groups is an indicator of the value of Ω_M, albeit somewhat biased to artificially low values (Frederic 1995b). The number density of dark matter halos as a function of their one-dimensional rms velocity dispersion, $n(\sigma_1)$, is an important test of the CDM clustering spectrum but here is used as a guide to whether the number of high velocity dispersion groups is reasonable. The ratio of the group-group autocorrelation, $\xi_{GG}(r)$, to the galaxy-galaxy autocor-

relation, $\xi_{gg}(r)$, is a test of biased clustering theory. Together these indicators provide valuable information as to whether galaxy groups have approximately the properties expected on the basis that the galaxies are orbiting in a dark matter–dominated potential that is at least partially virialized.

The derived group attributes come in three categories, with increasing sensitivity to the search parameters. First are the group centers, x, y, and z; second are the group projected size and velocity dispersion; and third are the specific galaxies in the groups. For all purposes the locations are key, whereas the extensions are secondary. The extensions do enter scaling relations, but whether individual galaxies are group members or not is irrelevant for our derivation of the mean internal properties of groups.

4.1. Virial Mass–to–Light Ratio

The ratio of the virial mass to the total luminosity, L_R^{ke}, is a valuable indicator of the CDM mass density of the universe. It does not measure any component of the mass that clusters weakly. The virial mass–to–light ratio of groups has quite considerable scatter simply as a result of both small number statistics and orbital projection. On the basis of dynamical simulations, Heisler, Tremaine, & Bahcall (1985) found that the dispersion in virial mass estimates as a result of these fluctuations is nearly a factor of 2 above and below the true mass, but this was comparable to other mass estimators. We calculate the virial mass, M_{VT}, using the galaxies in the groups with $r_p \le 1.5r_{200}$ and $\Delta v \le 3\sigma_1$, following the CNOC methods (Carlberg et al. 1996). That is,

$$M_{VT} = \frac{3\pi}{2G} \sigma_1^2 R_h , \qquad (2)$$

where the virial radius is evaluated for the galaxies identified as being group members. The circularly averaged harmonic radius is

$$R_h^{-1} = \left(\sum_i w_i\right)^{-2} \sum_{i<j} w_i w_j \frac{2}{\pi(r_i + r_j)} K(k_{ij}) , \qquad (3)$$

where $k_{ij}^2 = 4r_i r_j/[(r_i + r_j)^2 + s^2]$ and $K(k)$ is the complete elliptic integral of the first kind in Legendre's notation (Press et al. 1992). The softening, $s = 2''$, eliminates the divergence for galaxies at the same radius from the group center (Carlberg et al. 1996). The luminosity, L_R^{ke}, is k-corrected, evolution-compensated, and includes an extrapolation of the luminosity function to allow for galaxies below the redshift-dependent absolute magnitude cutoff. The evolution is taken to be at a mean rate of 1 mag per unit redshift.

If group galaxies are drawn from a universal luminosity function and the ratio of dark mass to luminous mass is a constant, then the median M_{VT}/L should be constant. The spread of the distribution of values can be used as an indicator of the statistical reliability of the group selection procedure. In Figure 3 we plot the median M_{VT}/L against the fractional difference between the first- and third-quartile M_{VT}/L values. In the same system clusters have $M_{VT}/L = 380 \pm 70$ $M_\odot/L_\odot$ (Carlberg et al. 1996), where we have removed the CNOC1 correction for the mean flattening of clusters. The median M_{VT}/L increases with both r_p^{max} and r_z^{max}. Groups selected with $r_p^{max} = 0.5$ h^{-1} Mpc and large r_z^{max} have huge median M/L values and a large spread between first- and third-quartile values, indicating that
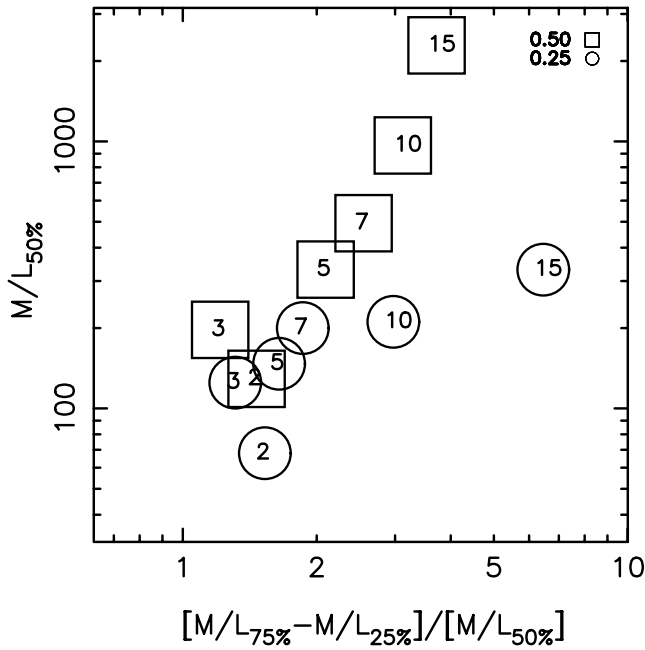
FIG. 3.—Median M/L value of the groups vs. the factional spread between the first- and third-quartile M/L values. Squares indicate $r_p^{max} = 0.5 \; h^{-1}$ Mpc groups, and circles indicate $r_p^{max} = 0.25 \; h^{-1}$ Mpc groups. The numbers in the symbols give the values of r_z^{max}.

these parameters are very poor choices for the identification of a uniform group population in this sample. Very small r_z^{max} lead to an increase in the spread and decrease in the mean M_{VT}/L. The origin of this decrease in M_{VT}/L with size is at least partially a result of the internal M/L gradient within groups that we discuss below. Overall, the $r_p^{max} = 0.25 \; h^{-1}$ Mpc groups with $r_z^{max} \leq 7 \; h^{-1}$ Mpc have the desirable property that both the spread and the median of the distribution do not change too much with r_z^{max}. We will settle on $r_p^{max} = 0.25 \; h^{-1}$ Mpc and $r_z^{max} = 5 \; h^{-1}$ Mpc for our "standard" groups. This is slightly arbitrary, with many of the properties of interest being insensitive to $\sim 30\%$ variations of the search parameters.

The derived properties of the groups have very substantial uncertainties because of the small number of galaxies with velocities. The errors in the velocity dispersion and the resulting correlation with the derived virial mass–to–light ratios are illustrated in Figure 4 for the $r_p^{max} = 0.25 \; h^{-1}$ Mpc and $r_z^{max} = 5 \; h^{-1}$ Mpc groups. The large velocity dispersion errors are the dominant source of the very strong correlation between the velocity dispersion and the derived M/L, as a consequence of M_{VT} being derived as $3G^{-1}\sigma_1^2 r_v$. This relation predicts the slope of the correlation visible in the figure. The inset diagram restricts the sample to groups with at least six members. For these larger groups the errors are somewhat less than the range of M/L, providing some support for a rising mass-to-light ratio with velocity dispersion.

4.2. The Number Density–Velocity Dispersion Relation

The number of groups as a function of their line-of-sight rms velocity dispersion is given in Figure 5 for a range of group search parameters. The median velocity dispersions for $r_p^{max} = 0.25 \; h^{-1}$ Mpc are 192, 229, 256, and 266 for r_z^{max} of 3, 5, 7, and 10 h^{-1} Mpc, respectively. Below 100 km s^{-1} is the regime of individual galaxies, which reduces the number

of groups relative to the number of dark matter halos at that velocity dispersion. These effects were anticipated within the simulated groups found within a mock redshift survey (Diaferio et al. 1999). An observational bias is that the velocity precision of the survey is about 100 km s^{-1}, which artificially reduces the number of low velocity dispersion groups. At this stage we recall that large values of the search length in the redshift direction tend to include enough outlier galaxies that a few groups are promoted into the high-σ_1 tail of the distribution. Given that high velocity dispersion groups also tend to contain the most galaxies (for a constant M/L), large groups are the easiest to find. Thus, low-membership groups with high velocity dispersions are likely to have erroneously large σ_1 values.

The Press-Schechter (1974) theory works well to describe the abundance of halos in n-body experiments and a range of observational data, including clusters over a range of redshifts (Carlberg et al. 1997b) and low-redshift groups (Girardi & Giuricin 2000). We can compare the Press-Schechter prediction for the number of groups to our observations. Because this requires absolute numbers, we will use the redshift range of greatest completeness, roughly 0.2–0.45.

To calculate the expected density, we follow the procedures outlined in Carlberg et al. (1997b) using $\Omega_M = 0.2$, $\Omega_\Lambda = 0$, and $\sigma_8 = 1.0$. We calculate the mass–velocity dispersion relation as

$$M_{1.5} = 8.6 \times 10^8 \sigma_1^3 \; M_\odot \; , \tag{4}$$

where σ_1 is given in units of km s^{-1} and the mass is the nominal value inside a virialized 1.5 h^{-1} Mpc sphere, as is appropriate for rich clusters, to which we want to normalize these predictions. The equivalent top-hat radius that contains this mass at the mean density is

$$R_L \simeq 8.43\Omega_z^{0.2p/(3-p)}\left(\frac{M_{1.5}}{6.97 \times 10^{14}\Omega_M h^{-1} \; M_\odot}\right)^{1/(3-p)}$$
$$\times (1+z)^{-p/(3-p)} \; h^{-1} \; \text{Mpc} \; , \tag{5}$$

where $p \simeq 0.64$ is the rate of increase of mass with radius (White, Efstathiou, & Frenk 1993; Carlberg et al. 1997b) and Ω_z is the value of Ω_M at redshift z. We evaluate the Press-Schechter relation as

$$n[M(\sigma_1)]dM = \frac{-3\delta_c(z)}{(2\pi r_L^2)^{3/2}\Delta}\frac{d\ln\Delta}{dM}\exp\left[-\delta_c^2(z)/2\Delta^2\right]dM \; , \tag{6}$$

where $\delta_c(z) = 0.15(12\pi)^{2/3}\Omega^{0.0185}/D(z, \Omega)$ (NFW96) and $\Delta(r_L)$ is the top-hat fractional linear mass variance in spheres of radius r_L calculated using a fitted CDM spectrum (Efstathiou, Bond, & White 1992). To determine the volume number density of halos for a finite range of velocity dispersion, we simply integrate over the relevant range of masses. Note that the normalization we have used automatically means that our group number densities will match on to the CNOC1 clusters (Carlberg et al. 1997b; Borgani et al. 1999; Girardi & Giuricin 2000).

The Press-Schechter predictions of number density for a median redshift of 0.36 are displayed in Figure 5. The subsample is contained in a volume of $1.8 \times 10^5 \; h^{-3}$ Mpc^3 (or about 50% more for a flat cosmology). Below 100 km s^{-1} the sample is missing many halos for two reasons. First, individual galaxy halos make up the majority of the halos in
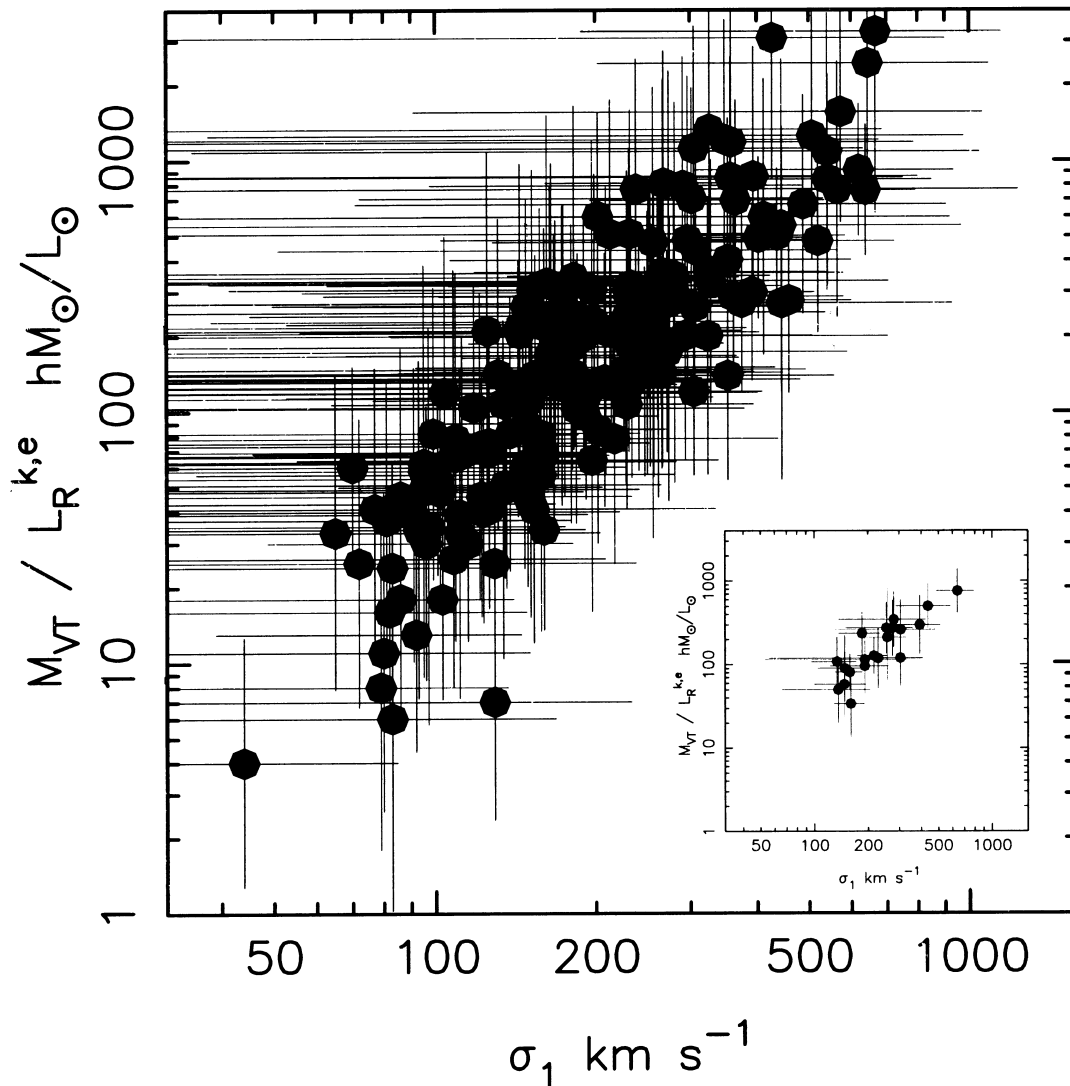
FIG. 4.—Mass-to-light ratios of the groups as a function of their velocity dispersions for $r_p^{max} = 0.25\ h^{-1}$ Mpc and $r_z^{max} = 5\ h^{-1}$ Mpc. The 1 σ error flags plotted are jackknife technique estimates. The correlation is the result of the σ_1^2 dependence of M_{VT}. The inset restricts the sample to groups with six or more members.

this regime. The velocity dispersion of an M_* elliptical is about equal to that of our median group (which in itself suggests an evolutionary connection). Second, because our velocity accuracy is about 100 km s^{-1}, low-velocity halos are scattered into the next higher bin. At this stage we recall that our expected completeness rate for higher velocity dispersion groups is about 50% and even lower for those with velocity dispersions comparable to individual galaxies.

The Press-Schechter predictions are in reasonable agreement with the groups for $r_z^{max} = 3$ and $5\ h^{-1}$ Mpc, bearing in mind that the random errors are at least $N^{1/2}$. Smaller values of r_z^{max} miss high-σ_1 groups, while larger values, $r_z^{max} \geq 7\ h^{-1}$ Mpc, produce a few highly improbable groups with the velocity dispersions of rich clusters.

There are three reasons to select the $r_p^{max} = 0.25\ h^{-1}$ Mpc and $r_z^{max} = 5\ h^{-1}$ Mpc groups as the best suited to our analysis of virialized halos with velocity dispersions of approximately 100–300 km s^{-1}, although other group selection parameters give rise to samples that show a very similar set of x, y, z locations. The selected groups have a relatively low dispersion in their M/L values, their $n(\sigma_1)$ distribution is close to the Press-Schechter prediction with

few high-velocity outliers, and the dynamical analysis below finds that our chosen redshift distance inclusion length pulls in most of the group members so that the derived velocity dispersions are fairly stable against the addition of more outlying members with increasing cutoff velocity.

4.3. The Two-Point Group-Group Correlation Function

A fundamental prediction of hierarchical dark matter clustering is that clustering, as measured by the two-point group-group correlation function $\xi_{GG}(r)$, should increase with the mass or velocity dispersion of the halo (Kaiser 1984; White et al. 1987). Here we measure both the redshift space correlation, $\xi(s)$, and the projected correlation function, $w_p(r_p)$, both of which provide an indication of the correlation length, r_0. The comoving redshift space separation is

$$s^2 = [r(\tfrac{1}{2}z_1 + \tfrac{1}{2}z_2)(\theta_1 - \theta_2)]^2 + [r(z_1) - r(z_2)]^2 , \quad (7)$$

with $r(z)$ being the comoving distance at redshift z. At separations small compared to the pairwise velocity converted to a distance, $\sigma_{12}/H(z)$, $\xi(s)$ ceases to increase with decreasing separation as the random velocities begin to
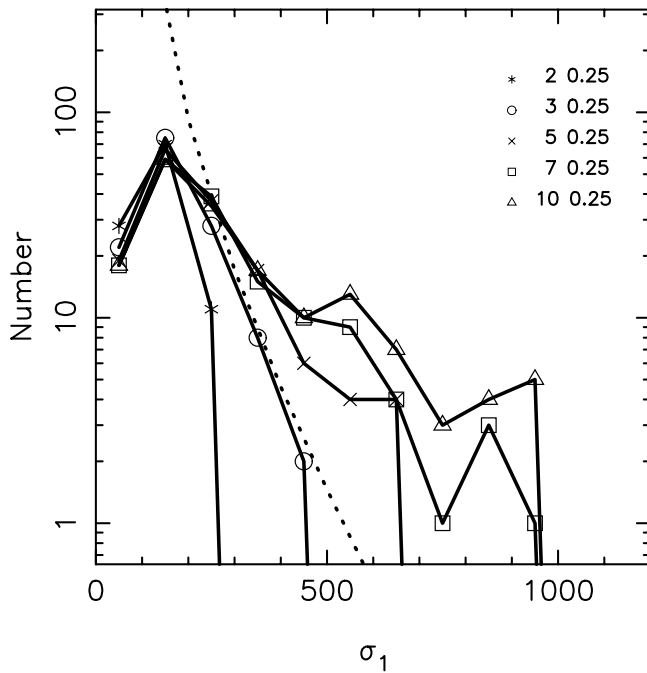
Fig. 5.—Distribution of measured line-of-sight velocity dispersions in 100 km s^{-1} bins, plotted at the bin centers. The parameters for the group selection are indicated by the symbols in the diagram. The dotted line shows the Press-Schechter prediction for the distribution using the cluster normalization.

Fig. 6.—Redshift space (*open circles*) and projected real-space (*filled circles*) correlations for the $r_p^{\mathrm{max}} = 0.25$ h^{-1} Mpc and $r_z^{\mathrm{max}} = 5$ h^{-1} Mpc groups. The errors here are simply the square root of the pair count in the bin. The fitted correlation lengths are 6.8 ± 0.3 and 6.5 ± 0.3 h^{-1} Mpc, respectively.

dominate the redshift space separation. On larger scales $\xi(s)$ is expected to be enhanced relative to $\xi(r)$ as a result of the "compression effect" of systematic infall (Kaiser 1987).

The projected correlation function, $w_p(r_p) = \int \xi[r_p^2 + r_z^2]^{1/2} dr_z$, has the advantage that the peculiar velocities have no effect on the result (Davis & Peebles 1983). We use the classical $DD/DR - 1$ estimator (Peebles 1980), which is suitable in the strong correlation regime. The random distribution is derived from a fit to the observed $n_g(z)$ distribution of the groups. Pairs are included for r_z up to 30 h^{-1} Mpc, comoving. For a power-law correlation function, $\xi(r) = (r_0/r)^\gamma$, the reduced projected correlation function, w_p/r_p, is equal to $A(\gamma)\xi(r)$, where $A(\gamma) = \Gamma(\frac{1}{2})\Gamma(\frac{1}{2}(\gamma - 1))/\Gamma(\frac{1}{2}\gamma)$, a factor of 3.68 for $\gamma = 1.8$ (Davis & Peebles 1983).

We evaluate the correlations using the same procedures and programs used in Carlberg et al. (2000) to measure the correlation of galaxies. Using the standard group sample ($r_p^{\mathrm{max}} = 0.25$ h^{-1} Mpc and $r_z^{\mathrm{max}} = 5$ h^{-1} Mpc), we evaluate $\xi(s)$ and $w_p(r_p)/r_p$ over the redshift range 0.15–0.55. We use as much redshift range as possible to boost the sample size. The resulting correlation functions are displayed in Figure 6. Note that the upward offset of $w_p(r_p)/r_p$ relative to $\xi(s)$ is a natural result of the $A(\gamma)$ factor. The error flags displayed in the figure are the square root of the number of galaxy pairs in each bin. Fitting the measured redshift space correlations to the function $\xi(r) = (s_0/r)^{1.8}$ gives $s_0 = 6.8 \pm 0.3$ h^{-1} Mpc. The fit of the projected correlation function yields $r_0 = 6.5 \pm 0.3$ h^{-1} Mpc. These errors are formal fitting errors and do not include an allowance for the patch-to-patch variance that likely dominates the random error.

The correlations measured for the CNOC2 galaxies over this redshift range in this cosmology have a mean of $r_0 = 4.2 \pm 0.2$ h^{-1} Mpc where this error includes the patch-to-patch variance (Carlberg et al. 2000). The ratio of the corre-

lation amplitude of our groups to that of the galaxies is 2.2 ± 0.4. At low redshift, Ramella, Geller, & Huchra (1990) found $s_0 \simeq 8$ h^{-1} Mpc for the CfA groups, which have a somewhat lower mean internal density than ours. A similar result emerged for the combination of the CfA and SSRS2 groups (Girardi, Boschin, & da Costa 2000), which found that the group correlation amplitude was a factor of 1.64 ± 0.16 stronger than that of galaxies, although by themselves the CfA groups were less biased relative to galaxies.
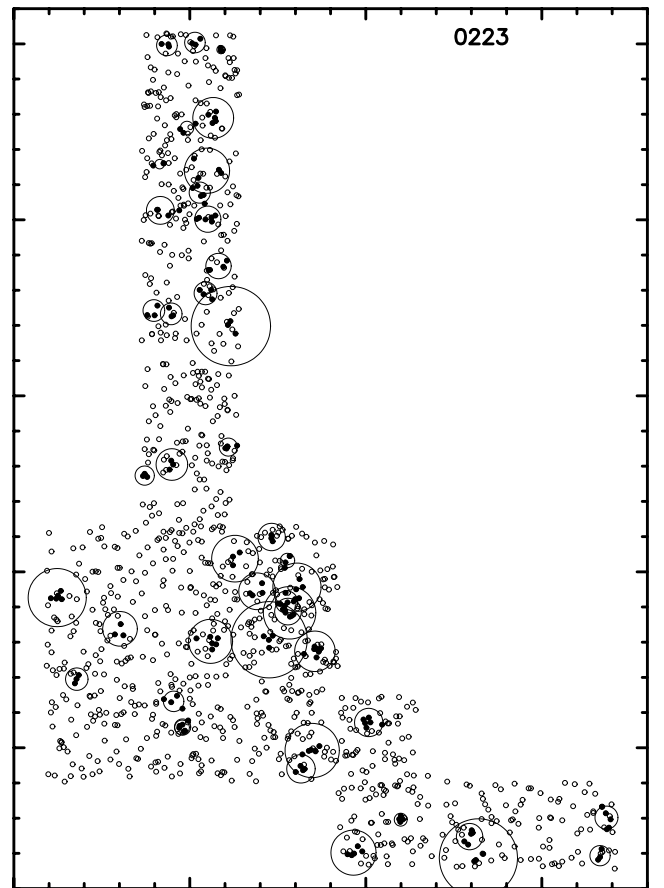
The biasing theory of Mo & White (1996) gives predictions of the expected ratio of correlation amplitudes. The characteristic velocity dispersion of normal galaxies is about 100 km s^{-1}, whereas our groups have a median velocity dispersion of about 200 km s^{-1}. From the CDM power spectrum (Efstathiou et al. 1992) with a shape parameter of $\Gamma = 0.2$, we calculate the linear mass variances to be 3.3 and 2.4 for 1 and 2 h^{-1} Mpc top-hat perturbations, which are approximately the unperturbed mean radii of the perturbations associated with galaxies and groups, respectively. With $\delta_c \simeq 1.68$ in the Mo & White (1996) model, we find that groups should be more strongly correlated by a factor of about 1.75 or 1.47 with the Jing (1998) n-body calibrated modification. Provided that the group velocity dispersion is about twice the galaxy velocity dispersion, the results are not very sensitive to the velocity dispersions chosen. We conclude that the correlation amplitudes are
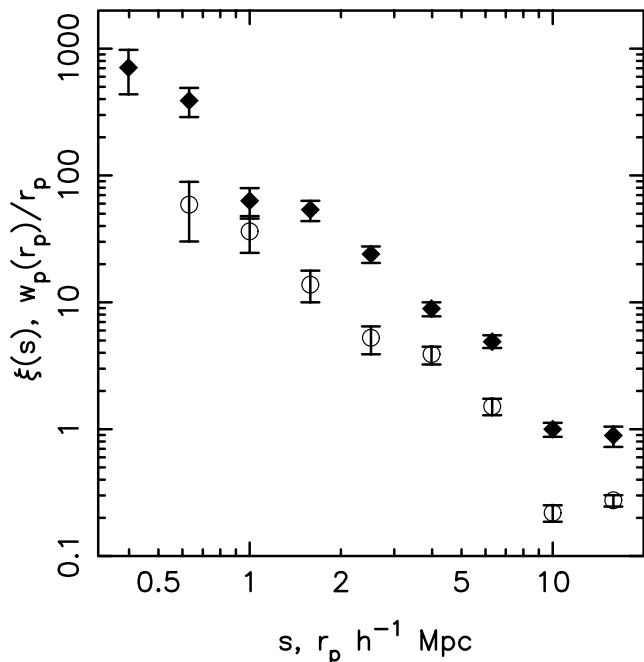
FIG. 7.—*xy* locations of field galaxies (*open circles*) and group galaxies (*filled diamonds*), along with r_{200} radii of the groups found between redshifts 0.1 and 0.45 in the 0223 + 00 field. The starting parameters are $r_p^{max} = 0.25\ h^{-1}$ Mpc and $r_z^{max} = 5\ h^{-1}$ Mpc (comoving). The group members are marked with filled symbols. Note that the group members fill their r_{200} to varying degrees. None of the members are outside the estimated region of virialization estimated for a low-density universe, $1.5r_{200}$. The major ticks are at intervals of 1000″, with north up and east to the left.

consistent with the expected relation at about the 1.5 σ level.

At this stage we have shown that our sample of groups is in good accord with three global statistics predicted on the basis of galaxies tracing CDM halos. The next issue is to examine the relative internal distribution of the dark matter relative to the galaxies.

4.4. The Adopted Standard Groups

The locations on the sky of the "standard" $r_z^{max} = 5\ h^{-1}$ Mpc and $r_p^{max} = 0.25\ h^{-1}$ Mpc groups for one of the patches are shown as the points in Figure 7. The circles indicate the r_{200} radii. Note that some groups are quite compact with respect to this radius. The parameters of all of the standard groups are given in Table 1. The columns give the sky location, redshift, σ_1 (from which r_{200} is calculated), the virial mass–to–light ratio, the number of group members with redshifts, and the mass. The random errors of the derived quantities, as estimated using the jackknife technique, are very large for most of the groups, a straightforward consequence of the small number of members.

5. MEAN INTERNAL STRUCTURE OF THE GROUPS

N-body simulations now have sufficient length resolution that they can reliably predict the highly nonlinear realization of the collapse of halos and their resulting internal density profile. A fundamental prediction is that CDM halos have a central density cusp, roughly $r^{-1.0}$ to $r^{-1.5}$ (Dubinski & Carlberg 1991; NFW96; Moore et al. 1999b; Avila-Reese et al. 1999). At large radii the density begins to drop as approximately r^{-3}. The characteristic radius of the density profile can be calibrated in *n*-body experiments and

derived from an approximate theory (NFW96). For the massive dark matter halos of rich clusters the NFW96 density function, $\rho(r) = Ar^{-1}(r + a)^{-2}$, is entirely consistent with the derived mass distribution (Carlberg et al. 1997a). The situation for galaxy mass halos is somewhat controversial, with constraining data coming from disk rotation curves in the presence of substantial amounts of baryonic mass and the modeling complication of partial pressure support relative to the circular velocity. However, there is evidence that in small velocity dispersion halos CDM may allow central densities that exceed the observations (Moore et al. 1999a, 1999b).

A fundamental difference between a galaxy and a rich cluster of galaxies is that galaxies have a strongly rising mass-to-light ratio with increasing distance from the center whereas rich galaxy clusters have a nearly constant mass-to-light ratio over their virialized volume (Carlberg, Yee, & Ellingson 1997c). Therefore, a basic question is whether groups exhibit a rising mass-to-light ratio. Individual groups have too few galaxies to make such a measurement. Moreover, groups come with a wide range of galaxy contents and have somewhat uncertain virialization because of their small numbers. Therefore, we effectively assemble a mean group to boost the numbers to levels where we can make reliable measurements of the density and velocity dispersion profiles.

5.1. The Group-Galaxy Two-dimensional Cross-Correlation Function

The group-galaxy cross-correlation function describes the average distribution of galaxies in a group in both radius and velocity. Precisely how the cross-correlation function is derived will have a significant impact on its properties. For instance, poorly determined centers will create a core in the projected profile, or superimposing a small low velocity dispersion group with a large high velocity dispersion group will lead to a rising velocity dispersion with radius. The idea is simple: we sum in projected radius and relative velocity around the group centers both the CNOC2 sample galaxies and a random sample drawn from the mean $n_g(z)$ (actually much larger than the galaxy catalog), then we subtract the randoms from the sample galaxies to give the excess. All galaxies are used, with no distinction given to galaxies that were used to define the group center. The group centers are determined in the virial analysis as the geometric weighted mean of the locations of the iteratively selected group members. We have adopted geometric weights, which help to compensate for the objects without redshifts. The smoothing radius used to calculate our geometric weights is 120″, which is so large that there is little weight variation within these small groups, but weights do vary from group to group. That is, at the x, y, z location of each of the n_G groups in turn, we count the number of galaxies in the neighborhood at separations r_p/r_{200} and $\Delta v/\sigma_1$, to measure the density distribution in redshift space of a group, $n_{Gg}(r_p, \Delta v)$. The density distribution is related to the two-dimensional group-galaxy correlation function, ξ_{Gg}, as

$$n_{Gg}(r_p, \Delta v) = n_G\, n_g(z) \left[\xi_{Gg}\left(\frac{R}{r_{200}}, \frac{\Delta v}{\sigma_1} \right) + 1 \right], \qquad (8)$$

where $n_g(z)$ is a smoothed fit to the redshift distribution locally converted to velocities in precisely the same way as

TABLE 1
The $r_z^{max} = 5\ h^{-1}$ Mpc, $r_p^{max} = 0.25\ h^{-1}$ Mpc Groups

R.A.	Decl.	z	σ_1 (km s^{-1})	M/L ($h\ M_\odot/L_\odot$)	N_g^z	M ($h^{-1}\ M_\odot$)
			0223+00			
02 23 21.9......	+00 43 10	0.12901	132 ± 71	135 ± 240	4	5.223E12 ± 97%
02 23 46.7......	+00 14 22	0.18809	80 ± 70	11 ± 36	3	5.116E11 ± 192%
02 23 42.5......	+00 29 59	0.19834	95 ± 74	58 ± 324	3	2.303E12 ± 127%
02 21 45.0......	−00 20 08	0.21787	126 ± 71	41 ± 61	5	3.443E12 ± 100%
02 23 29.3......	+00 47 14	0.22075	65 ± 68	33 ± 106	3	1.349E12 ± 183%
02 22 53.5......	+00 02 15	0.22781	111 ± 56	39 ± 56	4	3.995E12 ± 73%
02 23 04.5......	+00 03 18	0.22920	184 ± 50	206 ± 190	4	8.637E12 ± 48%
02 23 22.4......	−00 01 23	0.26741	254 ± 104	274 ± 283	6	2.084E13 ± 76%
02 20 53.1......	−00 18 28	0.27011	134 ± 38	108 ± 104	6	5.681E12 ± 74%
02 23 17.9......	+00 34 08	0.27038	148 ± 86	262 ± 433	4	7.775E12 ± 101%
02 20 55.7......	−00 22 04	0.27045	118 ± 123	104 ± 214	3	4.478E12 ± 137%
02 23 14.9......	+00 16 59	0.29864	115 ± 66	30 ± 44	5	1.704E12 ± 94%
02 24 20.3......	+00 02 53	0.30207	375 ± 85	271 ± 339	5	3.367E13 ± 43%
02 23 33.5......	−00 09 30	0.30275	95 ± 103	62 ± 108	3	1.541E12 ± 123%
02 23 36.5......	+00 55 06	0.30496	135 ± 130	51 ± 68	3	3.504E12 ± 115%
02 23 19.3......	+00 48 10	0.30520	266 ± 181	143 ± 202	5	1.619E13 ± 109%
02 23 12.8......	+00 06 24	0.30647	305 ± 326	1115 ± 2313	3	3.278E13 ± 150%
02 22 52.9......	+00 06 11	0.30933	95 ± 73	49 ± 74	4	2.304E12 ± 116%
02 22 11.0......	−00 18 28	0.33835	92 ± 53	13 ± 25	4	1.092E12 ± 165%
02 23 36.0......	+00 29 39	0.35084	160 ± 197	132 ± 406	3	5.871E12 ± 179%
02 23 33.3......	−00 09 28	0.35746	122 ± 112	46 ± 92	3	4.951E12 ± 113%
02 23 36.6......	−00 07 02	0.35772	154 ± 150	140 ± 279	4	1.130E13 ± 131%
02 23 00.2......	−00 01 17	0.35811	574 ± 483	1557 ± 2715	4	1.102E14 ± 117%
02 22 42.9......	−00 02 26	0.35851	305 ± 104	120 ± 139	7	2.441E13 ± 74%
02 22 49.5......	+00 03 39	0.36049	365 ± 169	693 ± 1044	5	6.553E13 ± 80%
02 22 52.9......	+00 01 21	0.36107	202 ± 68	85 ± 155	5	1.190E13 ± 62%
02 23 56.6......	−00 00 07	0.36464	265 ± 203	289 ± 498	3	3.008E13 ± 92%
02 22 29.1......	−00 21 32	0.38473	362 ± 218	287 ± 371	5	4.703E13 ± 88%
02 24 13.2......	−00 04 50	0.38483	180 ± 193	131 ± 345	3	8.168E12 ± 196%
02 22 22.8......	−00 09 13	0.38644	228 ± 173	119 ± 155	6	1.500E13 ± 104%
02 22 48.6......	−00 13 33	0.38661	229 ± 165	107 ± 172	4	1.064E13 ± 128%
02 23 21.7......	+00 38 35	0.39651	216 ± 42	127 ± 84	6	1.780E13 ± 35%
02 21 41.7......	−00 22 10	0.39654	645 ± 443	2439 ± 6437	3	1.521E14 ± 191%
02 23 36.3......	+00 15 23	0.39715	261 ± 211	264 ± 484	3	2.087E13 ± 103%
02 23 39.7......	+00 39 28	0.39785	230 ± 174	207 ± 170	4	2.036E13 ± 76%
02 23 22.9......	+00 31 34	0.40166	191 ± 92	128 ± 164	4	1.475E13 ± 66%
02 23 13.5......	+00 28 26	0.40494	667 ± 479	3266 ± 14005	3	1.799E14 ± 252%
02 22 44.3......	−00 11 49	0.40785	459 ± 141	277 ± 370	5	7.083E13 ± 54%
02 22 52.3......	+00 01 14	0.40816	444 ± 522	551 ± 1976	3	6.454E13 ± 231%
02 22 58.9......	+00 08 26	0.41259	234 ± 247	134 ± 196	3	1.003E13 ± 126%
02 23 24.7......	+00 41 07	0.41916	183 ± 60	140 ± 124	5	1.484E13 ± 50%
02 23 39.8......	+00 43 51	0.44237	86 ± 94	46 ± 132	3	2.524E12 ± 171%
02 23 25.9......	+00 55 19	0.46898	197 ± 142	64 ± 192	3	1.091E13 ± 92%
02 23 16.1......	+00 54 38	0.47066	79 ± 58	8 ± 28	3	7.906E11 ± 177%
			0920+37			
09 21 14.7......	+37 07 21	0.10712	103 ± 76	39 ± 146	3	2.583E12 ± 303%
09 18 04.3......	+36 55 28	0.11236	124 ± 89	40 ± 125	4	2.238E12 ± 144%
09 21 01.4......	+37 18 17	0.19117	253 ± 129	215 ± 550	5	1.928E13 ± 104%
09 20 26.0......	+37 35 55	0.19149	99 ± 82	82 ± 230	3	3.290E12 ± 109%
09 20 29.9......	+37 07 59	0.20203	108 ± 104	67 ± 299	3	3.422E12 ± 284%
09 21 24.8......	+36 59 29	0.20227	143 ± 163	124 ± 277	3	3.418E12 ± 146%
09 20 41.2......	+37 36 22	0.20714	262 ± 170	150 ± 343	4	1.120E13 ± 108%
09 17 24.4......	+36 54 14	0.22135	392 ± 120	299 ± 375	8	4.539E13 ± 70%
09 17 28.4......	+36 54 11	0.22476	164 ± 96	168 ± 302	4	1.029E13 ± 96%
09 17 18.9......	+36 54 00	0.22506	182 ± 188	342 ± 1308	3	1.077E13 ± 130%
09 17 24.6......	+36 56 39	0.22556	213 ± 255	509 ± 1235	3	1.584E13 ± 170%
09 20 56.8......	+37 19 35	0.23083	83 ± 54	24 ± 40	4	2.096E12 ± 114%
09 20 38.3......	+37 13 37	0.23299	197 ± 146	306 ± 889	3	1.046E13 ± 96%
09 20 57.5......	+37 06 49	0.24328	157 ± 104	223 ± 423	4	7.858E12 ± 105%

TABLE 1—*Continued*

R.A.	Decl.	z	σ_1 (km s^{-1})	M/L ($h\,M_\odot/L_\odot$)	N_g^z	M ($h^{-1}\,M_\odot$)
09 21 08.2......	+37 13 28	0.24347	202 ± 107	598 ± 947	4	$1.665\text{E}13 \pm 90\%$
09 20 54.9......	+37 21 12	0.24395	148 ± 43	90 ± 132	6	$7.245\text{E}12 \pm 59\%$
09 20 42.6......	+37 33 35	0.24438	185 ± 49	235 ± 192	6	$1.242\text{E}13 \pm 56\%$
09 20 15.5......	+37 19 47	0.24441	158 ± 27	81 ± 52	7	$6.221\text{E}12 \pm 42\%$
09 20 44.3......	+37 11 35	0.24447	125 ± 105	210 ± 866	3	$4.561\text{E}12 \pm 256\%$
09 21 02.7......	+37 23 11	0.24500	348 ± 329	1209 ± 2431	3	$3.154\text{E}13 \pm 118\%$
09 20 28.7......	+37 43 39	0.24515	297 ± 195	482 ± 1684	4	$2.833\text{E}13 \pm 94\%$
09 20 52.1......	+37 57 42	0.24535	226 ± 97	145 ± 157	5	$1.272\text{E}13 \pm 79\%$
09 20 33.7......	+37 49 38	0.24611	263 ± 58	337 ± 351	5	$2.289\text{E}13 \pm 46\%$
09 21 31.9......	+37 21 00	0.24623	147 ± 47	58 ± 83	6	$4.670\text{E}12 \pm 73\%$
09 20 26.0......	+37 22 44	0.24763	190 ± 107	199 ± 406	4	$1.366\text{E}13 \pm 119\%$
09 18 50.5......	+37 03 05	0.25424	97 ± 78	35 ± 180	3	$2.415\text{E}12 \pm 378\%$
09 20 38.1......	+37 30 33	0.25955	192 ± 139	114 ± 176	6	$1.369\text{E}13 \pm 119\%$
09 19 18.2......	+36 52 34	0.28641	72 ± 60	25 ± 69	3	$4.023\text{E}11 \pm 169\%$
09 20 36.0......	+37 29 37	0.31835	427 ± 473	3073 ± 8122	3	$9.172\text{E}13 \pm 152\%$
09 20 09.0......	+37 15 36	0.32181	144 ± 176	205 ± 649	3	$5.857\text{E}12 \pm 181\%$
09 20 53.5......	+37 44 31	0.32201	111 ± 93	33 ± 117	3	$2.974\text{E}12 \pm 113\%$
09 20 35.0......	+37 35 04	0.32273	167 ± 149	136 ± 367	4	$9.154\text{E}12 \pm 170\%$
09 20 24.0......	+37 24 48	0.32380	230 ± 113	305 ± 405	4	$1.378\text{E}13 \pm 98\%$
09 20 55.5......	+37 37 53	0.32384	256 ± 128	472 ± 543	5	$2.173\text{E}13 \pm 92\%$
09 20 42.9......	+37 30 05	0.36173	109 ± 92	66 ± 290	3	$4.329\text{E}12 \pm 312\%$
09 20 25.3......	+37 04 28	0.36178	412 ± 507	596 ± 1514	3	$3.697\text{E}13 \pm 181\%$
09 20 32.0......	+38 00 27	0.37218	542 ± 308	838 ± 1372	4	$5.252\text{E}13 \pm 117\%$
09 20 55.7......	+37 21 03	0.37237	160 ± 32	68 ± 79	4	$4.896\text{E}12 \pm 54\%$
09 20 53.7......	+36 58 08	0.37247	436 ± 148	502 ± 427	6	$5.015\text{E}13 \pm 56\%$
09 21 00.5......	+37 16 33	0.37291	126 ± 125	75 ± 128	3	$6.057\text{E}12 \pm 123\%$
09 21 11.8......	+37 03 14	0.37317	328 ± 210	360 ± 607	5	$4.321\text{E}13 \pm 95\%$
09 20 50.8......	+36 59 52	0.37323	251 ± 85	284 ± 425	4	$1.561\text{E}13 \pm 90\%$
09 21 12.5......	+37 15 50	0.37331	231 ± 129	287 ± 832	4	$1.720\text{E}13 \pm 197\%$
09 21 10.5......	+37 05 39	0.37352	147 ± 81	60 ± 81	4	$1.194\text{E}13 \pm 127\%$
09 21 02.2......	+37 02 00	0.37406	86 ± 82	43 ± 75	3	$2.761\text{E}12 \pm 113\%$
09 20 59.1......	+37 00 26	0.37426	639 ± 154	761 ± 628	8	$1.587\text{E}14 \pm 49\%$
09 20 49.6......	+37 21 49	0.37597	541 ± 506	1085 ± 2781	3	$6.384\text{E}13 \pm 125\%$
09 18 13.2......	+36 55 03	0.37893	109 ± 114	78 ± 240	3	$5.958\text{E}12 \pm 120\%$
09 19 38.6......	+37 10 04	0.37894	353 ± 246	402 ± 1069	3	$2.454\text{E}13 \pm 112\%$
09 19 13.9......	+37 01 54	0.37903	281 ± 224	298 ± 1408	3	$3.073\text{E}13 \pm 113\%$
09 20 45.7......	+37 29 04	0.37978	91 ± 102	39 ± 111	3	$2.769\text{E}12 \pm 121\%$
09 21 11.5......	+37 09 49	0.38032	328 ± 377	331 ± 677	3	$1.638\text{E}13 \pm 135\%$
09 21 02.8......	+37 40 03	0.38462	138 ± 104	82 ± 206	3	$9.262\text{E}12 \pm 177\%$
09 20 08.9......	+37 19 36	0.38820	403 ± 108	492 ± 542	4	$5.753\text{E}13 \pm 55\%$
09 19 25.3......	+36 56 23	0.38995	232 ± 191	510 ± 1099	3	$3.083\text{E}13 \pm 174\%$
09 20 33.9......	+37 25 10	0.39019	158 ± 122	56 ± 178	3	$4.814\text{E}12 \pm 112\%$
09 18 16.4......	+36 49 30	0.39096	184 ± 195	103 ± 192	4	$1.537\text{E}13 \pm 120\%$
09 20 03.7......	+37 21 26	0.39177	86 ± 54	18 ± 34	4	$2.451\text{E}12 \pm 109\%$
09 20 31.4......	+37 19 56	0.39196	209 ± 166	210 ± 573	3	$1.562\text{E}13 \pm 100\%$
09 21 13.0......	+37 21 06	0.39527	181 ± 199	142 ± 200	3	$5.827\text{E}12 \pm 122\%$
09 19 53.1......	+37 02 54	0.42748	102 ± 88	48 ± 76	3	$3.825\text{E}12 \pm 117\%$
09 19 18.9......	+36 49 49	0.46076	445 ± 484	270 ± 1094	3	$3.673\text{E}13 \pm 125\%$
09 21 06.9......	+37 21 05	0.46254	324 ± 379	200 ± 514	3	$3.258\text{E}13 \pm 171\%$
09 20 43.7......	+37 15 57	0.47277	294 ± 212	201 ± 430	3	$2.731\text{E}13 \pm 156\%$
09 21 28.5......	+37 14 48	0.47289	108 ± 100	26 ± 58	3	$2.635\text{E}12 \pm 114\%$
09 19 19.3......	+36 55 53	0.47318	353 ± 204	139 ± 223	4	$3.848\text{E}13 \pm 93\%$

1447+09						
14 47 15.9......	+09 15 08	0.16531	164 ± 126	322 ± 462	3	$1.263\text{E}13 \pm 126\%$
14 47 14.2......	+09 34 43	0.19733	233 ± 170	318 ± 543	4	$1.466\text{E}13 \pm 136\%$
14 47 21.9......	+09 52 00	0.20204	326 ± 360	1328 ± 3276	3	$2.271\text{E}13 \pm 151\%$
14 47 02.3......	+09 54 02	0.20249	250 ± 87	190 ± 438	4	$1.066\text{E}13 \pm 168\%$
14 47 27.0......	+10 01 43	0.22454	256 ± 280	248 ± 1706	3	$1.527\text{E}13 \pm 140\%$
14 47 11.9......	+09 50 10	0.22854	268 ± 107	811 ± 1911	4	$3.147\text{E}13 \pm 102\%$
14 47 20.6......	+09 41 36	0.22893	81 ± 98	37 ± 93	3	$2.308\text{E}12 \pm 165\%$
14 46 29.3......	+09 21 14	0.22897	162 ± 139	325 ± 1186	3	$7.214\text{E}12 \pm 113\%$
14 46 31.2......	+09 09 31	0.26162	229 ± 77	239 ± 668	4	$1.156\text{E}13 \pm 49\%$

TABLE 1—*Continued*

R.A.	Decl.	z	σ_1 (km s^{-1})	M/L ($h\,M_\odot/L_\odot$)	N_g^z	M ($h^{-1}\,M_\odot$)
14 47 01.7......	+09 04 18	0.26981	104 ± 92	119 ± 378	3	2.983E12 ± 132%
14 46 46.9......	+09 02 35	0.27057	112 ± 66	68 ± 132	4	3.020E12 ± 118%
14 46 36.0......	+09 01 42	0.27177	280 ± 143	347 ± 399	6	1.969E13 ± 85%
14 47 17.6......	+09 10 01	0.27286	165 ± 120	241 ± 732	3	8.104E12 ± 110%
14 47 58.8......	+09 23 48	0.28246	231 ± 116	187 ± 318	5	1.367E13 ± 80%
14 46 22.4......	+09 10 16	0.30639	93 ± 65	34 ± 126	3	1.329E12 ± 309%
14 47 53.9......	+09 18 22	0.30643	199 ± 161	228 ± 653	4	1.598E13 ± 103%
14 45 57.5......	+08 59 23	0.31031	83 ± 85	6 ± 29	3	6.854E11 ± 443%
14 45 46.5......	+09 07 56	0.32378	180 ± 149	181 ± 375	4	8.494E12 ± 145%
14 47 47.1......	+09 09 59	0.32506	175 ± 151	125 ± 214	4	9.875E12 ± 114%
14 47 28.5......	+09 31 36	0.32716	247 ± 148	144 ± 232	5	1.542E13 ± 96%
14 47 27.4......	+09 51 09	0.34855	136 ± 70	50 ± 76	6	4.741E12 ± 113%
14 47 19.1......	+09 43 26	0.35043	168 ± 169	200 ± 377	3	8.209E12 ± 120%
14 47 01.9......	+09 43 14	0.35062	250 ± 243	147 ± 239	3	1.893E13 ± 126%
14 46 37.1......	+09 19 28	0.35914	82 ± 66	16 ± 27	4	1.646E12 ± 127%
14 47 17.4......	+09 25 49	0.36192	170 ± 95	131 ± 183	5	9.828E12 ± 120%
14 47 41.1......	+09 23 57	0.36404	77 ± 94	41 ± 108	3	1.946E12 ± 173%
14 47 14.3......	+09 14 39	0.37225	126 ± 94	69 ± 153	3	2.787E12 ± 131%
14 47 56.3......	+09 13 36	0.37263	44 ± 41	4 ± 9	4	2.115E11 ± 154%
14 47 22.5......	+09 03 46	0.37389	291 ± 193	792 ± 1798	4	3.386E13 ± 158%
14 47 34.1......	+09 01 29	0.39369	308 ± 257	438 ± 535	4	3.596E13 ± 110%
14 46 47.7......	+09 23 40	0.39369	394 ± 406	864 ± 1972	3	4.819E13 ± 137%
14 47 28.8......	+09 08 34	0.39438	507 ± 469	1254 ± 2636	3	7.807E13 ± 114%
14 47 09.0......	+09 41 20	0.40653	101 ± 86	54 ± 76	3	3.620E12 ± 103%
14 46 12.9......	+09 03 31	0.46575	150 ± 146	118 ± 215	3	6.751E12 ± 122%
14 47 06.2......	+09 16 05	0.46820	488 ± 417	668 ± 1154	4	7.482E13 ± 125%
14 47 03.5......	+09 21 32	0.46930	217 ± 224	78 ± 166	4	8.894E12 ± 141%
14 47 04.9......	+09 17 29	0.47168	123 ± 99	40 ± 70	3	4.871E12 ± 121%
14 46 56.9......	+09 11 12	0.51077	565 ± 668	767 ± 1710	3	1.237E14 ± 149%
14 47 01.0......	+09 42 07	0.53680	520 ± 203	477 ± 625	5	1.355E14 ± 72%
14 46 57.1......	+09 07 42	0.54249	151 ± 132	63 ± 197	3	8.662E12 ± 177%
			2148−05			
21 48 18.9......	−05 59 04	0.12171	105 ± 110	91 ± 171	3	2.482E12 ± 120%
21 48 31.2......	−06 01 57	0.14300	140 ± 115	322 ± 724	3	6.164E12 ± 117%
21 48 01.4......	−06 00 20	0.14441	112 ± 72	54 ± 65	4	3.492E12 ± 81%
21 48 50.7......	−05 42 09	0.14467	137 ± 58	36 ± 70	5	7.359E12 ± 70%
21 48 49.9......	−05 33 03	0.14550	116 ± 87	29 ± 72	3	2.251E12 ± 95%
21 48 48.9......	−05 40 23	0.14644	235 ± 95	121 ± 275	5	1.230E13 ± 70%
21 48 43.3......	−05 21 24	0.14742	101 ± 48	35 ± 63	4	1.649E12 ± 124%
21 48 31.1......	−04 58 20	0.14908	219 ± 158	412 ± 893	4	2.253E13 ± 122%
21 48 35.8......	−05 02 09	0.15480	257 ± 76	211 ± 598	6	2.419E13 ± 71%
21 48 44.6......	−05 03 30	0.15649	241 ± 129	164 ± 298	4	2.631E13 ± 102%
21 48 53.9......	−06 04 10	0.17776	173 ± 193	167 ± 490	3	6.127E12 ± 124%
21 48 39.7......	−05 58 36	0.17803	238 ± 182	767 ± 1765	3	3.069E13 ± 100%
21 48 34.8......	−05 31 45	0.19828	267 ± 313	356 ± 1741	3	1.482E13 ± 439%
21 48 56.0......	−04 56 02	0.21406	152 ± 111	306 ± 611	3	1.124E13 ± 111%
21 49 07.6......	−05 47 27	0.21926	275 ± 81	273 ± 317	7	2.267E13 ± 65%
21 48 59.5......	−05 50 21	0.21940	192 ± 69	96 ± 80	6	5.039E12 ± 71%
21 48 58.1......	−05 45 07	0.21941	160 ± 31	34 ± 51	7	7.099E12 ± 52%
21 49 14.7......	−05 51 18	0.21964	96 ± 45	30 ± 75	4	1.494E12 ± 111%
21 48 11.3......	−06 05 54	0.23645	121 ± 90	73 ± 224	3	3.969E12 ± 218%
21 49 33.5......	−05 49 20	0.24135	149 ± 38	46 ± 59	5	3.683E12 ± 41%
21 48 55.1......	−05 21 45	0.24322	274 ± 168	316 ± 1951	4	3.163E13 ± 108%
21 48 52.4......	−05 10 11	0.24344	146 ± 114	113 ± 174	3	7.044E12 ± 124%
21 48 10.6......	−06 01 25	0.26489	306 ± 176	261 ± 334	6	3.355E13 ± 90%
21 48 29.9......	−04 59 18	0.28672	150 ± 74	111 ± 152	4	9.487E12 ± 65%
21 48 39.9......	−04 58 44	0.28792	144 ± 114	217 ± 751	3	9.609E12 ± 201%
21 49 34.2......	−06 06 33	0.30139	70 ± 50	60 ± 91	3	1.205E12 ± 93%
21 46 41.7......	−06 12 38	0.31265	103 ± 37	18 ± 27	5	1.161E12 ± 76%
21 48 31.7......	−05 02 41	0.31704	357 ± 394	853 ± 1720	4	6.038E13 ± 152%
21 48 19.7......	−05 54 31	0.31759	272 ± 318	173 ± 260	3	8.104E12 ± 123%
21 49 07.5......	−06 04 52	0.33391	131 ± 117	141 ± 445	3	6.826E12 ± 219%

TABLE 1—*Continued*

R.A.	Decl.	z	σ_1 (km s^{-1})	M/L ($h\ M_\odot/L_\odot$)	N_g^z	M ($h^{-1}\ M_\odot$)
21 46 13.5......	−06 09 28	0.35762	302 ± 230	705 ± 1242	4	5.002E13 ± 133%
21 47 58.5......	−05 55 41	0.35986	358 ± 428	1182 ± 3100	3	4.096E13 ± 162%
21 48 10.8......	−05 52 11	0.37338	174 ± 192	269 ± 394	3	1.064E13 ± 124%
21 47 51.8......	−05 55 23	0.39222	134 ± 107	49 ± 182	3	2.890E12 ± 213%
21 46 14.3......	−06 15 48	0.39364	214 ± 142	207 ± 379	4	1.986E13 ± 108%
21 48 43.7......	−05 09 11	0.39380	153 ± 181	41 ± 99	3	5.103E12 ± 140%
21 47 59.9......	−05 43 30	0.42607	129 ± 104	7 ± 14	4	1.492E12 ± 151%
21 48 07.3......	−05 55 27	0.44011	620 ± 314	915 ± 762	4	1.662E14 ± 60%
21 47 46.3......	−06 04 26	0.44041	208 ± 212	134 ± 293	3	2.160E13 ± 166%
21 48 05.2......	−05 42 26	0.46596	129 ± 109	25 ± 56	3	3.308E12 ± 167%

NOTE.—Units of right ascension are hours, minutes, and seconds, and units of declination are degrees, arcminutes, and arcseconds. Table 1 is also available in machine-readable form in the electronic edition of the *Astrophysical Journal*.

the real galaxy pairs. This is the $DD/DR - 1$ method (Peebles 1980) of calculating a cross-correlation between groups and galaxies. The correlation function ξ_{Gg} is the fundamental quantity of interest, since it has the background density removed. Both the surface density profile and the velocity dispersion profile are derived from ξ_{Gg}. Note that the total luminosity of the group uses the magnitude weights, which allows for the declining sampling rate toward the sample limit. Figure 7 builds the confidence that the selected centers are entirely sensible, although at this stage we cannot claim that this is an optimal procedure. Recalling that the group locations were not very sensitive to the details of the group finding, the resulting ξ_{Gg} is a reasonably robust quantity.

To derive the scaled group-galaxy cross-correlation, we will scale all the velocities to the σ_1 measured for each group and the radii to the r_{200} derived from the velocity dispersion. Because there is a substantial uncertainty in σ_1 for these small groups, these scalings contain a significant random element that is unavoidable. As the galaxies orbit in the groups, they will have different velocities and positions with time, which, because of the little averaging available in small groups, leads to considerable variation of their redshift space properties. Scaling the velocities and the radii avoids the pitfall of overlaying small low velocity dispersion groups on the inside and large high velocity dispersion groups on the outside, which would immediately lead to a rise of velocity dispersion with radius. The plot of the radial location of each galaxy that contributes to the mean group as a function of the source group's velocity dispersion in Figure 8 does show one potential systematic problem: the higher velocity dispersion groups do not extend out to $1.5r_{200}$. This suggests that redshift space interlopers are an important source of noise leading to velocity dispersions that are too large for the size of the group. To address this issue, we will also consider a number of alternate group samples.

Although these groups have small numbers of members, interlopers can be accurately removed statistically. We use the smoothed $n_g(z)$ that we derive from the galaxy sample as a whole using the procedures of our clustering analysis (Carlberg et al. 2000). The random catalog objects are scaled in precisely the same way as the true data to determine whether or not they are in the group. To do the subtraction, we need to bin the galaxies and randoms in r_p and Δv bins. We select bins that are 0.2 dex in $\log_{10}(r_p/r_{200})$ and

0.1 in the velocity scaled to σ_1. The binning is needed in our subsequent analysis anyway. We make velocity distance cuts at 3, 4, and 5 units as a check on the effect of residual interlopers and normally use the minimal noise 3 unit cut as our standard data set.

Although we have statistically subtracted the background from ξ_{Gg}, the velocity dispersion estimate is still sensitive to the presence of fluctuations in density at large velocity. In physical coordinates the densities of the groups are expected to be about $100\rho_0$ near r_{200}, but in redshift space this is reduced by a factor of roughly $3\sigma_1/[H(z)r_{200}] \simeq 20$ at our $\Delta v = 3\sigma_1$ cutoff. If there is a density normalization underestimate (overestimate), then the fraction of interlopers will increase (decrease) with r_p, since the contrast between the group and the surrounding field declines with increasing r_p. The probability of group interlopers can be estimated from the two-point correlation function. The probability that a galaxy with $r_p \le r_p^{\max}$ and
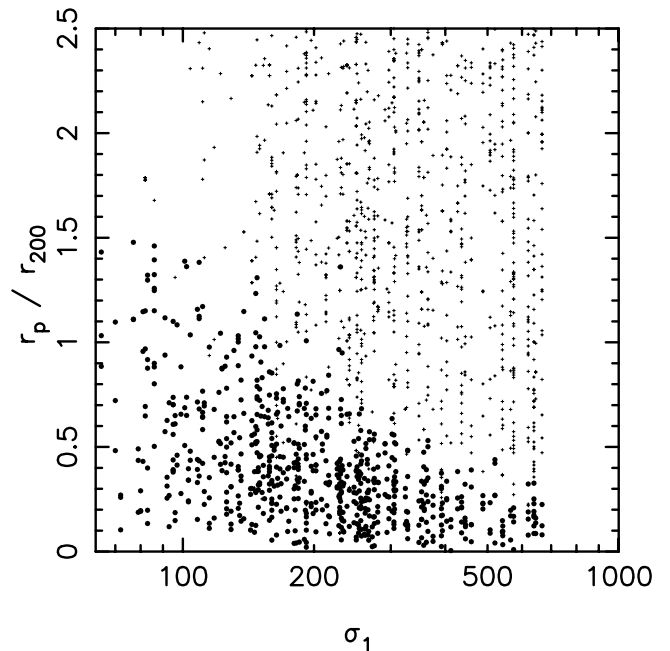

FIG. 8.—Scaled radius vs. the source group's velocity dispersion, using $\Delta v^{\max} = 3\sigma_1$. The small plus signs are for all galaxies contributing to ξ_{Gg}, whereas the filled octagons mark the galaxies identified as group members.

$\Delta v < \Delta v^{\mathrm{max}}$ is physically within $r < r_p$ is discussed in Carlberg et al. (2000). The conclusion is that slightly more than 50% of the galaxies within the required velocity separation are within the required radial separation, r. The other 50% are clustered toward the group but most probably at roughly a correlation length. Other than small factors of order unity, this redshift to real-space ambiguity always exists. This means that groups of size n may well be of size $n - 1$. The chance that they are of size $n - 2$ drops precipitously. Of course, as n rises, the fraction of interlopers is falling. These correlated but unvirialized group galaxies cannot be avoided. Although they present a challenge for a particular group, they are not a significant complication for most statistical analyses of the two-dimensional correlation function, given the density profile we derive below.

5.2. The Mean Density Profile

Integrating $\xi_{Gg}(r_p, \Delta v)$ over Δv gives the mean projected density profile displayed in Figure 9. The points are for cutoffs at 3, 4, and 5 velocity units, with the points declining slightly at small radii for increasing velocity cutoffs as a result of the normalization of the total integrated density to unity. The errors are evaluated from the patch-to-patch variance. There is little systematic change with increasing velocity cutoff. It is immediately clear that the projected density profile is very nearly a power law with only a weak break to a slightly shallower central profile. The mean projected slope of our virialized groups is approximately $\Sigma_N \propto R^{-1.5}$. To take into account the effect of Figure 8 that high velocity dispersion groups may be bogus, we restrict the sample to the $\sigma_1 \leq 200$ km s^{-1} groups. The result is shown
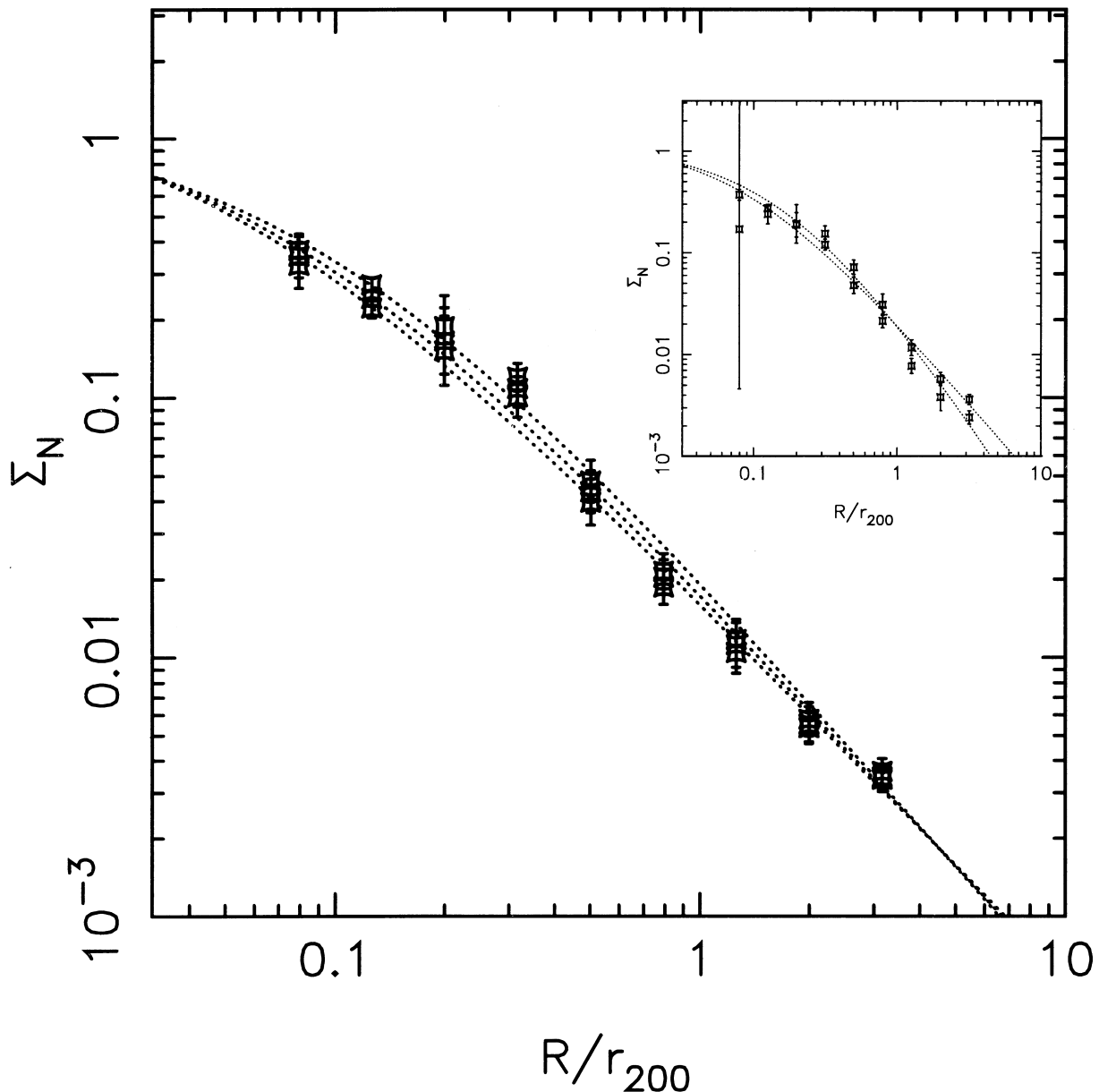
FIG. 9.—Number-weighted surface density of galaxies in the mean group. The points and three fitted lines show the slow *decrease* of the normalized surface density at intermediate radii with clipping at 3, 4, and 5 velocity units. The inset shows $\Sigma_N(R)$ using only the $\sigma_1 \leq 200$ km s^{-1} groups (*solid line*) and, for reference, all groups again (*dotted line*), adopting 3 velocity unit clipping in both cases.

in the inset to Figure 9. The density profile becomes somewhat steeper at large radii, and there is a suggestion that there is a break in the power law at small radii. The best-fit parameters are $a \simeq 0.7$ and $b \simeq 2.5$, although the core slope is not well defined.

We model the projected galaxy density distribution as the projection of the galaxy number density distribution,

$$v(r) = \frac{A}{4\pi r^a (r + c)^b} , \qquad (9)$$

which is projected to a surface density using

$$\Sigma_N(R) = 2 \int_R^\infty v(r) \frac{r}{\sqrt{r^2 - R^2}} \, dr , \qquad (10)$$

so that we minimize the variance in the $\Sigma_N(R)$ plane. The resulting best fit is degenerate because the scale radius is always found to be very small. For the data displayed we find $c = 0.061$, 0.074, and 0.062 for cutoffs of 3, 4, and 5, respectively. The $[a, b]$ pairs are $[0.50, 2.05]$, $[0.81, 1.71]$, and $[0.78, 1.71]$, respectively. However, other fits with $a + b = 2.55 \pm 0.05$ are equally acceptable given the small implied scale radius, c.

It is somewhat remarkable that, using our group centers, we identify such a cusped density profile. The procedure is not guaranteed to have any galaxy at the center of the group, whereas we find that on the average the galaxy density declines quite steeply away from the center. This is quite different from the cluster situation in which a similar average center gives a reduced central density (Carlberg et al. 1997c). The NFW96 profile does not provide a good fit to this distribution of galaxies, although it must be borne in mind that the NFW96 model describes the dark matter profile, not the galaxy distribution, which can in principle be quite different. Our observed group profile is near a power law that is steeper in the center and shallower at large radii than the NFW96 function or the steeper central cusps found by others (Moore et al. 1999a; Avila-Reese et al. 1999).

5.3. The Mean Velocity Dispersion Profile

The velocity dispersion profile allows the mass profile to be constrained. The projected velocity dispersion profile, $\sigma_p(R)$, for the $r_z^{\max} = 5 \ h^{-1}$ Mpc groups is shown in Figure 10. How robust is this rising $\sigma_p(R)$? Beyond about $2r_{200}$ there is no expectation that the galaxies are in virial equilibrium. The figure provides evidence that the slow rise in velocity dispersion across the virialized region is real and not a consequence of increasing interlopers with radius. Beyond about $2r_{200}$ virialized motions are small and the width of the distribution increases rapidly. The slow rise of $\sigma_p(R)$ is clearly rooted in the data, although a constant σ_p is not strongly excluded. It is well known that the pairwise velocity dispersion of galaxies has a similar weak rise with increasing separation; however, that is expected on the basis of the two-point correlation function falling as $r^{-1.8}$, rather than the $r^{-2.5}$ that we find here. A dynamical constraint from the Jeans equation is that, in a scale-free distribution, $\sigma^2 \propto \rho(r)r^2$. Therefore, the surprising outcome is the combination of the "steep" $\Sigma(R)$ and "slowly rising" $\sigma_p(R)$.

To evaluate the significance of the radial trends, we require reliable error estimates. The errors in $\Sigma(R)$ and $\sigma_p(R)$ are robustly and empirically evaluated from the patch-to-
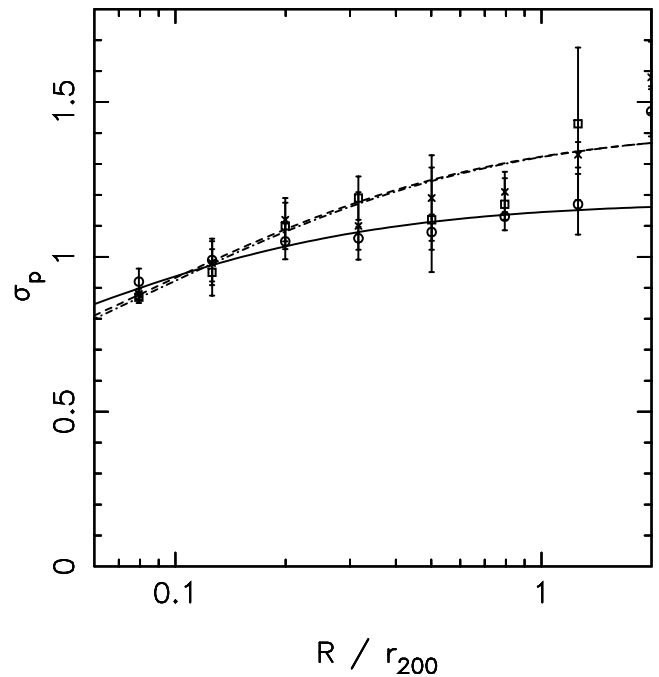

FIG. 10.—Number-weighted projected velocity dispersion profile. The circles, crosses, and squares are for velocity cuts at 3, 4, and 5 velocity unit cutoff, which are fitted by the solid, dashed, and dotted lines (virtually on top of each other).

patch variances in the quantities of interest. We find that the sensitivity to the velocity cutoff is relatively small, except that the errors increase in size. As a consequence, we will use the 3 velocity unit cutoff as our standard. The velocity dispersion is calculated as the second moment of the binned projected velocity distribution function (PVDF). Figure 11 displays the average PVDF, normalized to the velocity dispersion in each radial bin. We note that the observed PVDF is much closer to Gaussian than to an exponential, although relative to the Gaussian the group mean PVDF appears to have a small excess at small and large velocities. This PVDF indicates that only mild anisotropy is allowed (van der Marel et al. 2000), at least for simple distribution functions.

The projected velocity dispersion is easily modeled as the projection of a three-dimensional velocity dispersion, where we adjust the radial velocity dispersion, $\sigma_r(r)$, and the velocity anisotropy, $\beta(r)$, to fit the data. The projection integral is

$$\sigma_p^2(R)\Sigma_N(R) = \int_R^\infty v(r)\sigma_r^2 \left[1 - \beta(r)\frac{R^2}{r^2}\right] \frac{r}{\sqrt{r^2 - R^2}} \, dr . \qquad (11)$$

N-body models suggest that the orbits of galaxies should be similar to that of the full dark matter distribution, with some deficiency of radial orbits that are selectively removed as a result of merging and tidal destruction (Ghigna et al. 1998). In principle, the velocity ellipsoid is constrained by the PVDF, shown in Figure 11.

We model the radial velocity dispersion as

$$\sigma_r^2(r) = \frac{Br}{b + r} , \qquad (12)$$

which is a solution of the Jeans equation that worked well for clusters (Carlberg et al. 1997c). In the absence of other
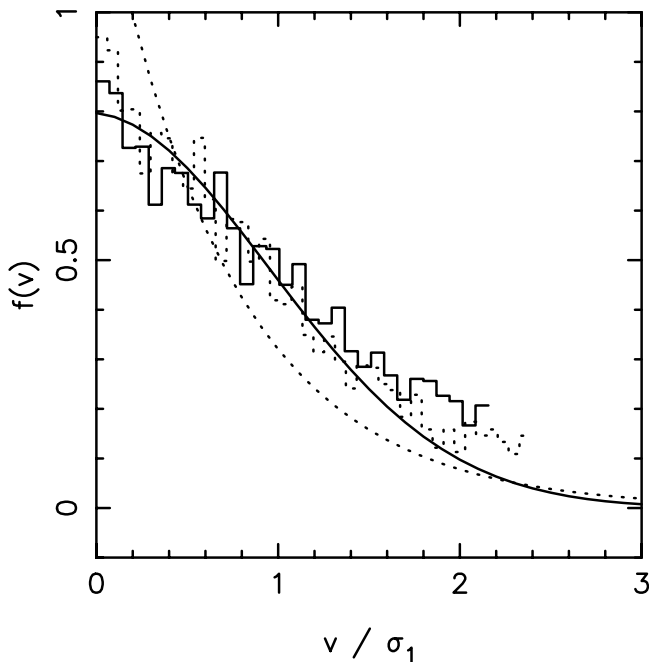
FIG. 11.—PVDF, normalized to have unit velocity dispersion and unit area under the curve. The PVDFs for cutoffs of 3 and 4 velocity units are shown as solid and short-dashed stepped lines, respectively. The reference lines are a Gaussian (*solid line*) and an exponential distribution (*short-dashed line*).

information, the velocity anisotropy, $\beta = 1 - \sigma_\theta^2/\sigma_r^2$, is best taken to be a constant independent of radius. However, that choice immediately leads to the somewhat surprising result that the mass-to-light ratio rises with radius. In order to investigate the sensitivity of the result to the velocity anisotropy, we adopt the model

$$\beta(r) = \beta_0 \, w(r) + \beta_\infty [1 - w(r)] \,, \tag{13}$$

where $w(r) = r_\beta^2/(r_\beta^2 + r^2)$. This $\beta(r)$ function goes to β_0 at the origin and β_∞ at large radius. As reasonable alternatives we set $r_\beta = 0.1r_{200}$ or $0.3r_{200}$. This parameter could in principle be part of the nonlinear fit, but because dynamical problems are underconstrained without some knowledge of the velocity anisotropy, we choose to use values of this parameter where our $\beta(r)$ gives a useful variation over the range of the data. The fits are shown for the three different velocity cutoffs in Figure 10. Note that the results for different β are essentially indistinguishable and that the model has little difficulty giving a statistically acceptable fit to the data.

6. THE RISING MASS-TO-LIGHT RATIO

The dynamical mass profile can be derived from the tracer density profile, $v(r)$, its velocity dispersion, $\sigma_r(r)$, and the velocity anisotropy, $\beta(r)$, using the Jeans equation,

$$M(r) = -\frac{\sigma_r^2 r}{G} \left(\frac{d\ln \sigma_r^2}{d\ln r} + \frac{d\ln v}{d\ln r} + 2\beta \right). \tag{14}$$

The validity of this equation does not rely on $v(r)$ being distributed like the mass density, $\rho(r)$. It does require that the system be in dynamical equilibrium, which our group selection procedures are specifically designed to pick out. Throughout we will use $L(r) = 4\pi \int vr^2 \, dr$ as the luminosity

profile, assuming that galaxies have the same mean luminosities at all radii. Strictly speaking we are working out the mass-to-number ratio. The assumption that low- and high-luminosity galaxies are similarly distributed relative to the mass field is explicitly tested below. The advantage of this approach is that it weights the galaxies relatively equally, rather than concentrating most of the statistical weight on the high-luminosity galaxies.

In Figure 12 we display the $M(r)/L(r)$ profile for the standard group centers with the velocity dispersion calculation cutoff set at 3 velocity units. Note that this shows the integrated interior M/L, not the local values. We first model these groups using a conventional approach with minimal anisotropy. That is, the central velocity ellipsoid is isotropic, i.e., $\beta_0 = 0$, and the anisotropy radius, r_β, is at about the midpoint of the virialized region, $r_\beta = 0.3r_{200}$. The outer anisotropy, β_∞, takes on the values -1, $-\frac{1}{2}$, 0, and $\frac{1}{4}$, which range from nearly tangential to slightly radial velocity anisotropy. The M/L curves are normalized to unity at the data point closest to $r/r_{200} = 1$. The data indicate about a factor of 3–10 rise in the mass-to-light ratio per decade of radius, with little sensitivity to the outer velocity anisotropy. That is, the light is much more centrally concentrated than the mass. This effect is visible for many of the groups where their sky distribution is much more concentrated than their r_{200} as shown in Figure 7.

The insets in Figure 12 address the concern about erroneously large σ_1 values biasing the properties of the mean groups. The lower inset shows the results of the analysis based on the groups restricted to have five or more members. The upper inset is the result of the analysis where we have overlaid all groups in physical coordinates. For easy comparison to the other figures we have taken $\sigma_1 = 200$ km s^{-1} so that all quantities can be scaled as before. Although there are differences in the details of the resulting M/L curves, the rising trend is preserved. Both of these alternative group samples indicate that the rise in the mass-to-light ratio is not as large as the scaled results of the full group sample would indicate. However, the situation remains unclear since the $N \geq 5$ groups tend to have higher velocity dispersions and overall M/L values (Fig. 4), which leads us to expect that effects that drive segregation will be smaller.

The mass density profile, $\rho(r)$, derived from the mass profile as $(4\pi r^2)^{-1} dM/dr$, is plotted in Figure 13 for the same models as in Figure 12. The model with the most extreme velocity ellipsoid at large radii, the tangentially dominant $\beta_\infty = -1$ (*solid line*), implies a large core that becomes relatively smaller as β_∞ becomes more positive. This model-dependent result is one of the most interesting aspects of these groups, and its reality needs to be tested, which we can at least partially do within our own data. The upper inset is for the $N \geq 5$ sample analyzed in coordinates scaled to r_{200}. The lower inset shows the results based on a two-dimensional correlation function in physical coordinates, where we have normalized to a $\sigma_1 = 200$ km s^{-1} group. Neither of these alternatives gives rise to significantly different results. The existence of a core in the dark matter distribution depends sensitively on the assumption that the velocity anisotropy is close to isotropic. A strong tangential anisotropy in the center, $\beta_0 = -1$, is able almost to eliminate the mass-to-light gradient. However, we recall that the PVDF of Figure 11 does not favor such strong anisotropy.
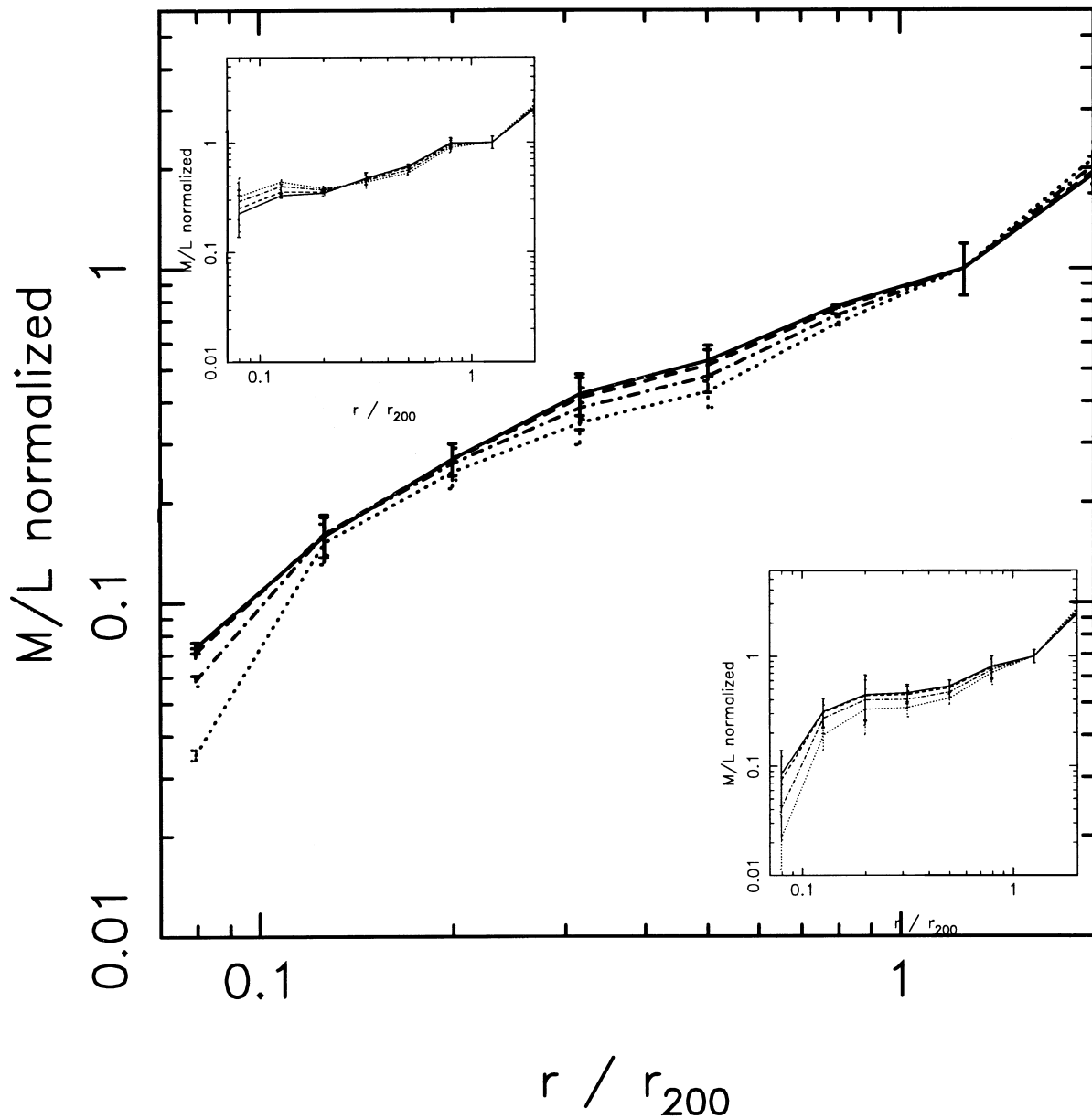
FIG. 12.—Rising mass-to-light ratio from the 3 velocity unit cutoff velocity dispersion profile for group centers identified with $r_p^{max} = 0.25\ h^{-1}$ Mpc and $r_z^{max} = 5\ h^{-1}$ Mpc. The galaxy coordinates are scaled to their groups σ_1 and r_{200}. The errors are computed from the velocity dispersion errors. The upper inset shows the results obtained by overlaying the galaxies in physical coordinates assuming $\sigma_1 = 200$ km s^{-1}, and the lower inset shows the results after restricting the analysis to groups with five or more members The solid, dashed, dot-dashed, and dotted lines are for $\beta_\infty = -1,\ -\frac{1}{2}, 0$, and $\frac{1}{4}$, respectively.

The source of the rising M/L in the kinematic data is readily understood. In a power-law density distribution with a radial density dependence of $\rho \propto r^{-2+p}$, the mass generating the potential must have a velocity dispersion profile of $\sigma^2 \propto r^p$. From the velocity dispersion we measure that $p \simeq \frac{1}{4} \pm \frac{1}{4}$. This implies a mass density profile that is slightly shallower than r^{-2}. The measured mean light profile $v(r) \propto r^{-2+q}$, with $q \simeq -\frac{1}{2}$. Consequently, the mass-to-light ratio, $\int \rho r^2\ dr / \int v r^2\ dr$, which varies as r^{p-q}, rises as $r^{3/4 \pm 1/4}$. Nearly circular orbits can flatten the M/L profile for the observed velocities, but these β would be very different from the observational results for rich galaxy clusters (Carlberg et al. 1997c; van der Marel et al. 2000) and n-body experiments (Ghigna et al. 1998). One significant difference between groups and rich clusters is that the timescale for dynamical friction to act declines as σ_1^3, so that dynamical

friction is much more effective for galaxies orbiting in groups than for clusters.

7. DISCUSSION AND CONCLUSIONS

In this paper we use the CNOC2 survey catalogs, containing approximately 6000 galaxies with redshifts, restricted to an $M_R^{ke} \leq -18.5$ mag sample of 3290 galaxies from which we identify more than 200 high-probability virialized groups. These groups contain, on the average, 3.8 redshift members (the sample is not complete) for a total of about 800 group members with redshifts. This represents about 21% of all eligible galaxies in the approximately volume-limited galaxy sample. These groups have selection-dependent M_{VT}/L values comparable to the values of large clusters with the "standard" groups being about a factor of 2 lower. The group population volume density matches on
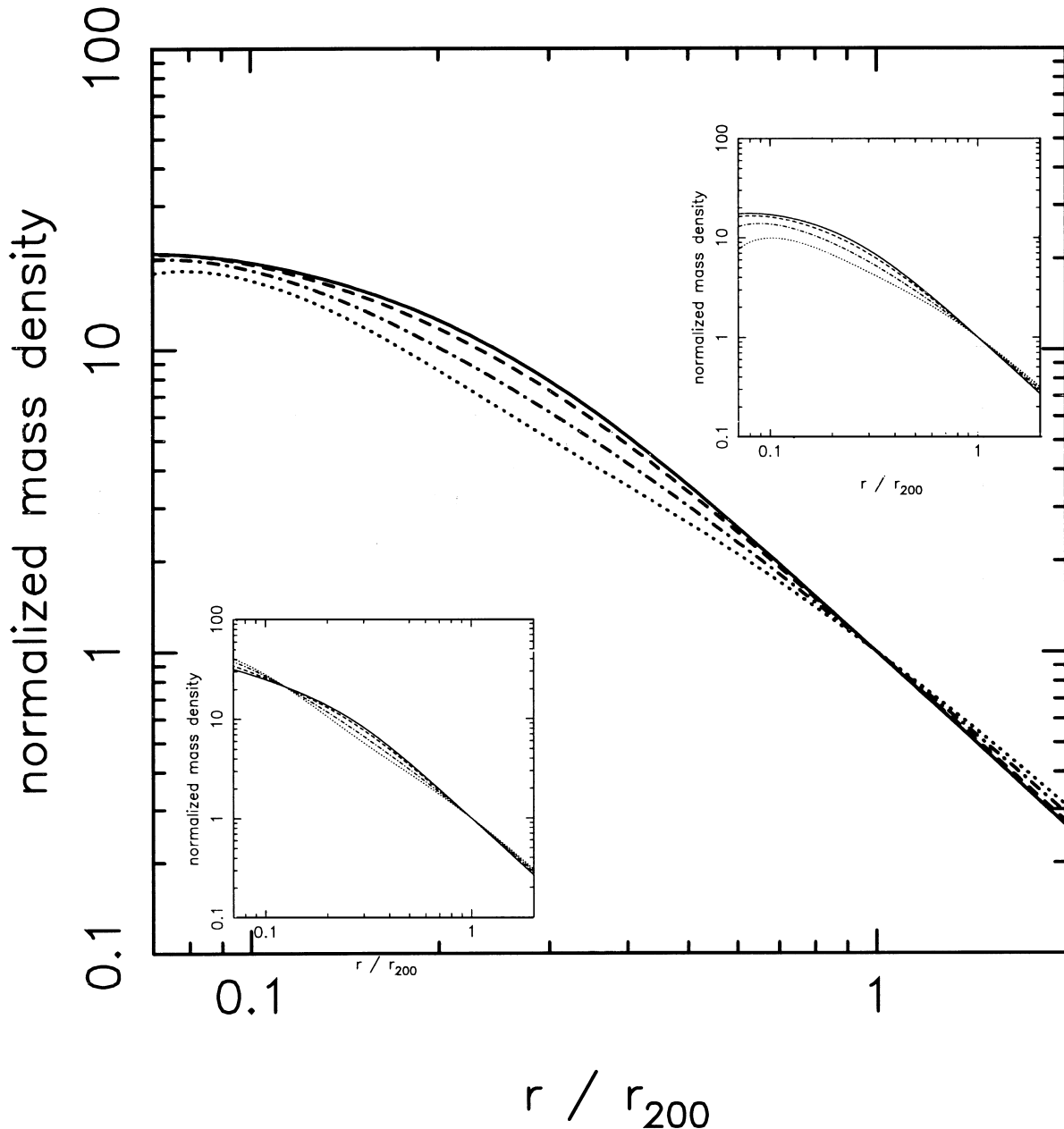
FIG. 13.—Inferred dark matter density profile for the variable velocity anisotropy model, with $\beta_0 = 0$, $r_\beta = 0.3r_{200}$, and $\beta_\infty = -1$, $-\frac{1}{2}$, 0, and $\frac{1}{4}$ for solid, dashed, dot-dashed, and dotted lines, respectively, as in Fig. 12. The lower inset shows the results obtained by overlaying the galaxies in physical coordinates, and the upper inset shows the results after restricting the analysis to groups with five or more members.

to the number–velocity dispersion relation of clusters above about 200 km s^{-1}. Lower velocity dispersion groups appear to be deficient relative to the Press-Schechter prediction. The clustering of groups is enhanced at about the level expected for the approximately 200 km s^{-1} velocity dispersion dark matter halos of groups as compared to the approximately 100 km s^{-1} halos of individual galaxies. Overall the global properties of groups are about as expected for dark matter halos on this mass scale.

Quite unlike rich clusters, which have a mass-to-light profile constant with radius (Carlberg et al. 1997c), our analysis of the internal properties of galaxy groups finds considerable evidence for a gently rising mass-to-light profile with radius. We argue that the rising velocity dispersion profile with radius is not an artifact of the analysis; however, this inference depends on the theoretical and indi-

rect observational indication that the mean velocity ellipsoid is approximately isotropic. Hence, this result needs to be independently verified. Current indirect support for this result comes from X-ray observations of low-redshift galaxy groups having velocity dispersion overlap with our sample near 300 km s^{-1}. The X-ray emission is significantly more extended than most of the group light, indicating a rising M/L (Kriss, Cioffi, & Canizares 1983; Mulchaey & Zabludoff 1998). Weak gravitational lensing is one of the best prospects to check this result since it has no dependence on assumptions of equilibrium. These intermediate-redshift groups are ideally situated for weak lensing studies (H. Hoekstra et al. 2001, in preparation). The somewhat puzzling weak lensing results for the low velocity dispersion cluster MS 1224+20 in two independent studies indicate that the M/L is rising with radius (Fahlman et al. 1994;

Carlberg 1994; Fischer 1999). Given the large group-to-group fluctuations, it will be important to examine a statistically meaningful sample.

Assuming that the rising M/L is real, the most likely physical explanation is that galaxies sink with respect to the dark matter via dynamical friction. It is important to note that near r_{200} both the galaxies and the dark matter have undergone about the same amount of collapse relative to the field. It is only in the inner third or so where the major differences develop, and the size of those differences is strongly dependent on the kinematic model. As galaxies cluster together to form a group, their individual halos are tidally removed to join the common halo from the outside in. Dynamical friction from the collisionless dark matter causes the galaxies to sink in the common group halo, over about a Hubble time (Barnes 1985; Mamon 1987; Evrard 1987; Bode, Cohn, & Lugger 1993; Pildis, Evrard, & Bregman 1996). One possible concern with this interpretation is that when groups join together to make rich clusters this history needs to be erased to leave no M/L gradient, at least as measured with the current precision. Furthermore, whether this mechanism is consistent with no luminosity dependence of the M/L gradient but with a large galaxy color dependence of the M/L gradient puts some fairly strong, but not necessarily unreasonable, constraints on the formation history of the galaxies.

A more extreme possibility for the origin of the M/L gradient is that the dark matter is subject to some effective pressure that does not allow it to undergo full gravitational collapse to form a core, either through a phase density limit or through collisional interactions (Spergel & Steinhardt 2000). More conventional explanations should be carefully examined and our results independently verified with other methods of observation before this is accepted.

REFERENCES

Abell, G. O. 1958, ApJS, 3, 211
Avila-Reese, V., Firmani, C., Klypin, A., & Kravtsov, A. V. 1999, MNRAS, 310, 527
Barnes, J. 1985, MNRAS, 215, 517
Bode, P. W., Cohn, H. N., & Lugger, P. M. 1993, ApJ, 416, 17
Borgani, S., Girardi, M., Carlberg, R. G., Yee, H. K. C., & Ellingson, E. 1999, ApJ, 527, 561
Burbidge, E. M., & Burbidge, G. R. 1961, AJ, 66, 541
Carlberg, R. G. 1994, ApJ, 434, L51
Carlberg, R. G., et al. 1997a, ApJ, 485, L13
Carlberg, R. G., Morris, S. L., Yee, H. K. C., & Ellingson, E. 1997b, ApJ, 479, L19
Carlberg, R. G., Yee, H. K. C., & Ellingson, E. 1997c, ApJ, 478, 462
Carlberg, R. G., Yee, H. K. C., Ellingson, E., Abraham, R., Gravel, P., Morris, S., & Pritchet, C. J. 1996, ApJ, 462, 32
Carlberg, R. G., Yee, H. K. C., Morris, S. L., Lin, H., Hall, P. B., Patton, D., Sawicki, M., & Shepherd, C. W. 2000, ApJ, 542, 57
Davis, M., & Peebles, P. J. E. 1983, ApJ, 267, 465
Diaferio, A., Kauffmann, G., Colberg, J. M., & White, S. D. M. 1999, MNRAS, 307, 537
Diaferio, A., Ramella, M., Geller, M. J., & Ferrari, A. 1993, AJ, 105, 2035
Dubinski, J., & Carlberg, R. G. 1991, ApJ, 378, 496
Efstathiou, G., Bond, J. R., & White, S. D. M. 1992, MNRAS, 258, 1
Eke, V. R., Navarro, J. F., & Frenk, C. S. 1998, ApJ, 503, 569
Evrard, A. E. 1987, ApJ, 316, 36
Fahlman, G., Kaiser, N., Squires, G., & Woods, D. 1994, ApJ, 437, 56
Fischer, P. 1999, AJ, 117, 2024
Frederic, J. J. 1995a, ApJS, 97, 259
———. 1995b, ApJS, 97, 275
Ghigna, S., Moore, B., Governato, F., Lake, G., Quinn, T., & Stadel, J. 1998, MNRAS, 300, 146
Girardi, M., Boschin, W., & da Costa, L. N. 2000, A&A, 353, 57
Girardi, M., & Giuricin, G. 2000, ApJ, 540, 45
Gott, J. R., III, & Turner, E. L. 1976, ApJ, 209, 1
Heisler, J., Tremaine, S., & Bahcall, J. N. 1985, ApJ, 298, 8
Hickson, P. 1982, ApJ, 255, 382
Huchra, J. P., & Geller, M. J. 1982, ApJ, 257, 423

Jing, Y. P. 1998, ApJ, 503, L9
Kaiser, N. 1984, ApJ, 284, L9
———. 1987, MNRAS, 227, 1
Kriss, G. A., Cioffi, D. F., & Canizares, C. R. 1983, ApJ, 272, 439
Lin, H., Yee, H. K. C., Carlberg, R. G., Morris, S. L., Sawicki, M., Patton, D., Wirth, G., & Shepherd, C. W. 1999, ApJ, 518, 533
Mahdavi, A., Böhringer, H., Geller, M. J., & Ramella, M. 2000, ApJ, 534, 114
Mahdavi, A., Geller, M. J., Böhringer, H., Kurtz, M. J., & Ramella, M. 1999, ApJ, 518, 69
Mamon, G. A. 1987, ApJ, 321, 622
Mo, H. J., & White, S. D. M. 1996, MNRAS, 282, 347
Moore, B., Frenk, C. S., & White, S. D. M. 1993, MNRAS, 261, 827
Moore, B., Ghigna, S., Governato, F., Lake, G., Quinn, T., Stadel, J., & Tozzi, P. 1999a, ApJ, 524, L19
Moore, B., Quinn, T., Governato, F., Stadel, J., & Lake, G. 1999b, MNRAS, 310, 1147
Mulchaey, J. S., & Zabludoff, A. I. 1998, ApJ, 496, 73
Navarro, J. F., Frenk, C. S., & White, S. D. M. 1996, ApJ, 462, 563 (NFW96)
Nolthenius, R., & White, S. D. M. 1987, MNRAS, 225, 505
Peebles, P. J. E. 1980, Large Scale Structure of the Universe (Princeton: Princeton Univ. Press)
Pildis, R. A., Evrard, A. E., & Bregman, J. N. 1996, AJ, 112, 378
Press, W. H., & Schechter, P. 1974, ApJ, 187, 425
Press, W. H., Teukolsky, S. A., Vetterling, W. T., & Flannery, B. P. 1992, Numerical Recipes in C (Cambridge: Cambridge Univ. Press)
Ramella, M., Geller, M. J., & Huchra, J. P. 1989, ApJ, 344, 57
———. 1990, ApJ, 353, 51
Spergel, D. N., & Steinhardt, P. J. 2000, Phys. Rev. Lett., 84, 3760
van der Marel, R. P., Magorrian, J., Carlberg, R. G., Yee, H. K. C., & Ellingson, E. 2000, AJ, 119, 2038
White, S. D. M., Davis, M., Efstathiou, G., & Frenk, C. S. 1987, Nature, 330, 451
White, S. D. M., Efstathiou, G., & Frenk, C. S. 1993, MNRAS, 262, 1023
Yee, H. K. C., et al. 2000, ApJS, 129, 475